A new finite element axisymmetric model with non-axisymmetric thermal loads for thermal analyses of tread braked wheels

Tribology International 209 (2025) 110675

Contents lists available at ScienceDirect

Tribology International

journal homepage: www.elsevier.com/locate/triboint

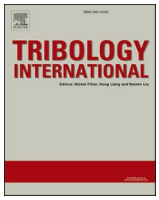

A new finite element axisymmetric model with non-axisymmetric thermal loads for thermal analyses of tread braked wheels

Matteo Magelli, Nicolò Zampieri *

Politecnico di Torino, Department of Mechanical and Aerospace Engineering, C.so Duca degli Abruzzi 24, Torino 10129, Italy

ARTICLE INFO

Keywords:
Tread braking
Railways
Finite element method
Fourier series

ABSTRACT

The paper describes the implementation of a finite element (FE) model for the calculation of the temperature field on tread braked wheels in ANSYS Mechanical APDL. The model is based on axisymmetric-harmonic elements, that allow to apply non-axisymmetric thermal loads over an axisymmetric geometry, thanks to the definition of thermal loads in terms of Fourier series coefficients. The model is benchmarked against a reference 3D model, in steady-state and transient simulations, and it provides the same outputs with improved computational times and management of memory resources. As the new model has 390 fewer degrees of freedom with respect to the 3D model, speed up factors around 1580 can be achieved, and smaller step-sizes are enabled.

1. Introduction

The typical braking system adopted on most freight wagons is tread braking, based on brake blocks with friction material shoes pushed against the wheel tread surface with a mechanical leverage system [1], as sketched in Fig. 1. Simple design and low costs are the two great advantages of tread braking. However, the mechanical power of the braked vehicles is dissipated into friction heat, which flows into the wheel and is responsible for high local temperatures, especially during drag braking operations, i.e., when the vehicle is coasting on a downhill track section.

The temperature rise occurring on the outer surface of tread braked wheels is responsible for wheel steel softening, with consequent wheel distortions, plastic deformations, and deterioration of the wheel-rail contact performances [2]. At the same time, the local temperature peaks can give rise to residual thermal stresses, that are known to have a detrimental effect on the fatigue behaviour of the wheel steel [3]. Moreover, due to the working principle of tread braking, a point on the wheel tread outer surface is subjected to friction heating followed by cooling mainly due to convection with ambient air and partially by radiation for the remaining part of the wheel revolution. Previous literature [4] has shown that this can cause local microstructural changes in the wheel steel, with the subsequent generation of additional stresses and an undesired excess of brittle behaviour. Unfortunately, these phenomena are favourable to thermal crack nucleation and propagation, and the combination of tread braking with wheel-rail contact stresses is known to exacerbate the rolling contact fatigue (RCF) and tread wear phenomena [5–7]. The latter can eventually result into shelling, spalling and even wheel warping, which can lead to an increase of the derailment risk [8–12].

The concern on the damage sources related to tread braking has strongly raised with the introduction of composite shoes [13,14], especially LL-type shoes, replacing traditional cast-iron shoes (P10 shoes), which were known to cause high levels of rolling noise [11,15]. In fact, these engineered materials have a lower thermal conductivity, which causes a bigger amount of friction heat to flow into the wheel, hence exacerbating the previously mentioned thermally induced damages. Furthermore, the adoption of new shoe materials is generating some apprehension, shared by other braking systems, about friction material wear and particulate matter (PM) emissions, which depend on temperature and can have a negative impact on human health and the environment [16–18].

Numerical models able to estimate the temperature field in tread braked wheels could lead the path towards tuning monitoring algorithms for early detection of surface damage phenomena, hence reducing the high costs of maintenance operations with an optimized intervention scheduling. Furthermore, efficient numerical models could allow to assess the performances of engineered composite friction materials with respect to the previously mentioned concerns, and even to identify optimal braking strategies. All these goals can be achieved through innovative strategies in the literature, based on including computationally efficient thermal models of wheels and brake blocks directly within longitudinal train dynamics (LTD) or multibody (MB)

* Corresponding author.
E-mail address: nicolo.zampieri@polito.it (N. Zampieri).

https://doi.org/10.1016/j.triboint.2025.110675
Received 16 January 2025; Received in revised form 17 March 2025; Accepted 26 March 2025
Available online 29 March 2025

List of Symbols

Latin Alphabet

c	Specific heat
D	Thermal conductivity matrix
F_{air}	Braking force on vehicle
F_N	Brake block pressing force
$F_{N,max}$	Brake block pressing force
F_{ord}	Ordinary resistant force
F_{res}	Total resistant force
g	Gravity acceleration
h	Summation counter
H(·)	Heaviside function
i_s	Track slope
K	Thermal stiffness matrix
$\mathbf{K_D}$	Stiffness matrix due to conduction
$\mathbf{K_\alpha}$	Stiffness matrix due to convection
M	Specific heat matrix
M_{tot}	Total weight on rails
N	Maximum order of retained harmonics
N_{ax}	Number of axles
N_{bw}	Number of blocks per wheel
N	Matrix of shape functions
$\mathbf{N_{axsym}}$	Matrix with shape functions depending on axial and radial coordinates
$\mathbf{N_{78}}$	Matrix of shape functions for ANSYS PLANE78 element type
P	Period of a function
P_{ax}	Vehicle axle-load
$\mathbf{Q_\alpha}$	Vector of convection loads
$\mathbf{Q_\Phi}$	Vector of convection loads
r	Radial coordinate
R	Rotation matrix
S	Surface
S_2	Domain border with prescribed heat flux
S_3	Domain border with prescribed convection
t_{fill}	Brake cylinder filling time
T	Temperature
T	Vector of harmonic temperature
T_B	Bulk temperature of surrounding fluid
$\mathbf{T^n}$	Vector of nodal temperatures
v	vehicle speed
V	Volume
z	Axial coordinate

Greek Alphabet

α	Convection coefficient
δ	Virtual
Δθ	Relative rotation
λ	Thermal conductivity
η	Natural coordinate along axial direction
θ	Angular coordinate
Θ	Matrix of harmonic functions
Θ_0	Angular width of the shoe
μ_{wb}	Wheel-shoe friction coefficient
ξ	Natural coordinate along radial direction
ρ	Density
τ	Brake cylinder filling constant
Φ	Heat flux
Φ	Heat flux matrix
Φ'	Heat flux matrix after rotation
Φ_{unit}	Fourier series coefficient for unitary flux
Φ*	Average heat flux flowing into the wheel
$\widetilde{\Phi}_w$	Fourier series of heat flux flowing into the wheel

Subscripts

h	Summation counter
l	Summation counter
w	Wheel

Superscripts

a	Anti-symmetric
m	Symmetry counter
n	Nodal
s	Symmetric
t	transposition

List of Abbreviations

1D	Mono-dimensional
2D	Bi-dimensional
3D	Three-dimensional
BC	Boundary condition
Bg	Bremsklotz geteilt (one shoe per block holder)
CAD	Computer aided design
DOF	Degree of freedom
FD	Finite difference
FE	Finite element
HAE-NAL	Harmonic axisymmetric element with non-axisymmetric loads
LTD	Longitudinal train dynamics
MB	Multibody
OS	Operating system
o.w.	Otherwise
PM	Particulate matter
RCF	Rolling contact fatigue
TSI	Technical specifications for interoperability

codes, to output temperatures whilst performing dynamic simulations [19–21].

Tudor et al. [22] developed an analytical model for the calculation of the steady-state temperature field of a wheel braked by two blocks to calculate the heat flux partitioning at the wheel-rail and wheel-shoe contact interfaces, but this model is only valid for a perfectly cylindrical wheel, and it cannot be adopted to evaluate the evolution of the thermal field in transient operations. Due to the simplifying hypotheses of analytical models and thanks to the computational power of modern computers, most of the thermal models for tread braked wheels in the literature are based on numerical methods, with the finite element (FE) method being the most widespread, although some examples of finite difference (FD) method exist [23]. The literature review suggests that there are mainly three types of modelling strategies, namely i) pure axisymmetric models, ii) 3D models and iii) models in the radial-circumferential plane. Axisymmetric models, with the one developed by Swedish researchers [24–26] being a milestone in the field, are the most common strategy, as they allow to reduce the computational effort by only defining elements and nodes on a wheel section. Nonetheless, pure axisymmetric models only predict the average temperature along the wheel circumferential direction, which makes it impossible to detect the temperature variation and fast cooling occurring during a wheel revolution. However, to account for higher temperature peaks in the circumferential region where the wheel contacts the block, Vernersson et al. [24] calculated a local temperature rise as the steady-state solution of an analytical 1D model. This temperature rise was superimposed to the uniform temperature computed with the axisymmetric model for the evaluation of the heat flux repartition

between the wheel and blocks. Similarly, Vakkalagadda et al. [27] developed a FE axisymmetric model with a uniform spreading of the friction heat flux along the wheel circumferential direction, but they partitioned the heat developed at the wheel-shoe and wheel-rail interfaces according to the results of a boundary element model considering the radial and circumferential coordinates. Recently, Siniscalchi and Cantone [23] validated a 2D axisymmetric FD mode and benchmarked it against the model by Vernersson et al. [24].

To account for the non-axisymmetric heat flux along the circumferential coordinate and enable the detection of local temperature peaks, different authors have built FE models of the wheel and/or brake block in the radial-circumferential plane. Teimourimanesh et al. [28] built a plane circumferential model with the goal of investigating the hot spot phenomenon, modelling the wheel as a thin ring to consider fewer degrees of freedom (DOFs). Babu and Prasad [29] built a FE model in ANSYS for the evaluation of the wheel and shoe temperature field along the radial and circumferential directions and meshed the model with elements performing a weak coupling between the mechanical and thermal DOFs, thus solving the wheel-shoe contact at each time-step. Nonetheless, they found that the contact pressure distribution is approximately unchanged during the braking operation. Bosso et al. [30] developed a similar model, which completely decouples the mechanical and thermal problems, implementing independent mechanical and thermal modules. The mechanical module solved the wheel-shoe contact problem, considering friction and sliding at the contact interface. On the other hand, the thermal module was used to calculate the wheel temperature field, further reducing the number of DOFs by only modelling 1/8 of the wheel and applying consistent boundary conditions (BCs) at the symmetry edges. However, the main drawback of plane circumferential models is that they often assume plane stress conditions when solving the mechanical contact problem, thus specifying a constant or unitary thickness in axial direction and not modelling with enough accuracy the wheel section geometry. This also hinders from properly applying convective BCs on all surfaces, and this issue can only be partially mitigated with approximated approaches based on global energy balances.

The highest modelling accuracy can be achieved with FE models meshing the whole wheel with 3D solid elements, hence being able to easily calculate the temperature in each circumferential position. This modelling strategy has the great advantage of simple implementation in commercial codes, as the mesh can be defined on the geometry imported from detailed CAD drawings. Milosevic et al. [31] modelled the wheel geometry in SOLIDWORKS and ran transient thermal simulations with COMSOL, while Pradhan and Samantaray [32] used the ABAQUS software package. The ABAQUS code was also adopted by Haidari et al. [33,34], who meshed the wheel with elements coupling thermal and mechanical behaviour to investigate the fatigue life of cracked wheels, modelling in detail the wheel-rail contact problem. Despite the ease of implementation and the high accuracy, 3D FE models are computationally demanding, with computational speeds slower by more than one order of magnitude when compared to equivalent 2D axisymmetric models as proved by Yevtushenko et al. [35].

As highlighted in the lines above, 3D models can predict the thermal field in tread braked wheels with the highest accuracy and account for all nonlinearities, but they are characterized by a high computational burden. Conversely, 2D axisymmetric and plane models reduce the computational costs because they have a smaller number of DOFs. Nonetheless, pure axisymmetric models cannot capture the temperature variation along the circumferential direction, thus only providing the average temperature for each wheel revolution, while plane models hinder from the proper application of all BCs and thermal fluxes.

To combine the excellent computational performances of 2D axisymmetric models with the capabilities of 3D models of estimating the temperature variation along the circumferential direction, this paper implements a new FE model built as an ANSYS APDL routine and based on plane harmonic axisymmetric element with non-axisymmetric thermal loads (2D HAE-NAL model). The main advantage of this ANSYS library element lies in the application of non-axisymmetric BCs over the axisymmetric geometry of the wheel, using Fourier series coefficients for the definition of the non-axisymmetric thermal load components. Therefore, as un upgrade of existing axisymmetric models reviewed above, the 2D HAE-NAL model can calculate the temperature field as a function of the circumferential coordinate as well. Although Fourier series are a well-known mathematical technique and harmonic elements accepting non-axisymmetric loads are already available from the library of commercial FE packages, the application of such modelling strategy for the calculation of the temperature field in tread braked wheels is a novelty in the literature, to the authors' knowledge.

A huge point of merit of the adopted approach is that the temperature field is obtained as the superposition of different orders and functions (sine or cosine) in the Fourier series, which can be solved independently. Therefore, the selected modelling strategy virtually enables a full parallelization of the computation, thus requiring a simulation effort well comparable with the one required by traditional axisymmetric models. The greatest advantages of the 2D HAE-NAL model are related to the capability of predicting the temperature filed along the circumferential direction while at the same time modelling and meshing the wheel section geometry only, thus reducing the number of DOFs and consequently increasing the computational efficiency. Please note that, although the present paper mainly focuses on tread braked wheels, the mathematical formalism described in the Sections below can be adapted to any practical application where non-axisymmetric thermal loads act on axisymmetric bodies, such as for disc brakes [36] but also cutting discs of tunnel boring machines [37–39].

The objective of the paper is to describe the mathematical foundation of the 2D HAE-NAL model and its implementation within the ANSYS APDL FE code, as well as to benchmark it against an easier-to-implement

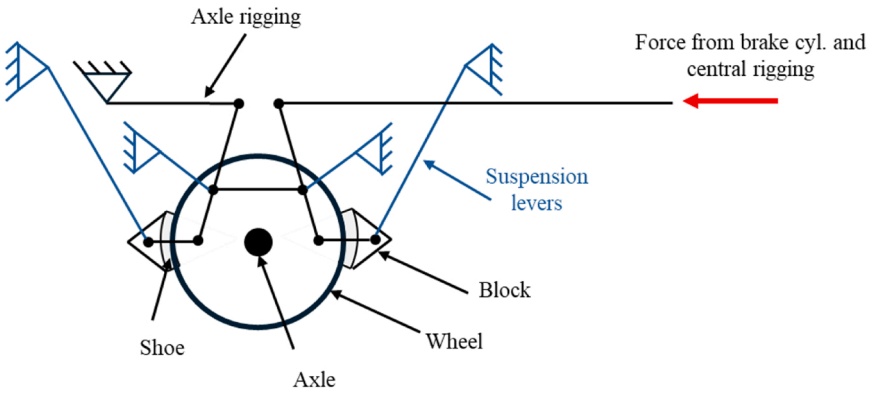

Fig. 1. Tread braked wheel (2Bg configuration).

but computationally expensive 3D model, whose outputs are taken here as a reference. The experimental validation of the model is outside the scope of the paper, and it is going to be faced in future upgrades of the activity, as the authors' research group has been currently upgrading the design of a new scaled twin-disc rig [40] to carry out laboratory tests to assess the thermo-mechanical behaviour of railway wheels.

The motivation behind this work lies in the need for a computationally efficient thermal model that can be useful for the investigation of different temperature-related phenomena, such as wheel tread wear and crack initiation/propagation, PM emissions, noise, etc. Furthermore, the benchmarked 2D HAE-NAL model will serve as a foundation for the development of an in-house simplified 1D model that will be implemented within the computational framework of MB codes, thus enabling the investigation of the mutual effects between vehicle dynamics and wheel-shoe contact temperature.

The paper is structured as follows. Section 2 provides the mathematical background of the modelling approach adopted for the 2D HAE-NAL model and describes the implementation of the developed models in the ANSYS Mechanical FE code, using the APDL environment for the new 2D HAE-NAL model and the Workbench package for the 3D reference model. Section 3 shows the validation of the 2D HAE-NAL model, presenting the results of preliminary simulations. Finally, the Conclusions section summarizes the main outcomes of the activity discussing the main benefits of the newly developed model.

2. Material and methods

At the current stage of the activity, the 2D HAE-NAL model is implemented in the ANSYS APDL package, but it can be implemented in any in-house FE code based on the mathematical formalism described in the rest of this Section. The new 2D HAE-NAL model is validated against a detailed 3D model meshing the wheel with solid elements and built in ANSYS Workbench. Both the 2D HAE-NAL and the reference 3D model are developed as purely thermal models, having temperature as the only DOF in their nodes. The underlying assumption, which is consistent with the findings of paper [29] and is often adopted in the literature for other types of braking system as well [41,42], is that the structural and thermal DOFs can be solved independently, thus speeding up the simulation times. Nonetheless, the models can account for the effective heat flux distribution derived from the contact pressure calculated with a separate structural contact model specifically implemented to solve the wheel-shoe contact problem, as already done by the authors in [30]. Therefore, the distribution of the heat flux flowing into the wheel at the contact with the shoe must be fed to the developed models as the major input.

The simulations shown in this work are launched considering a constant heat flux in the wheel-shoe contact region and the common 2Bg block configuration, i.e., each wheel is braked with two blocks featuring a single friction material shoe each, see the sketch in Fig. 2a). However, the adopted modelling approach is not restricted to consider any specific block configuration or heat flux distribution, as different conditions can be simulated with a consistent adjustment of the model inputs. Furthermore, since the primary goal of the paper is the description of the benefits brought by the new 2D HAE-NAL model, an approximated geometry, see Fig. 2b), is considered for the wheel section. This choice is explicitly made to simplify meshing operations and the application of BCs, thus favouring the comparison between the two models and avoiding discrepancies due to meshing of complex geometries when using the two packages. However, the modelling approach can be easily extended to consider any desired wheel profile, web and hub shape. As noticeable from Fig. 2b), the wheel tread geometry is modelled in a simplified manner and a constant radius is assumed on the outer surface. However, the model can be easily upgraded in future developments to consider the real wheel profile, so it can be adapted to consider a variation of radius along the axial coordinate, thus accounting for variable peripheral speed and hence friction heat flux distribution along the tread.

Both the 2D HAE-NAL model and the reference 3D model consider the friction heat flux flowing into the wheel in the tread region of the wheel outer surface where the contact with the shoes occurs, while on all free surfaces, convection cooling with the ambient air is applied. Radiation is currently not applied in the models, since its contribution in typical tread braking operations is assumed to be negligible with respect to the frictional heat flux and air convection. Nonetheless, the models can be upgraded in the future to account for this contribution. Finally, on the inner surface (bore diameter) conduction towards the wheel axle is prescribed, with the latter modelled as a mass with large thermal capacitance, whose value is estimated from typical dimensions of railway axles adopted on European freight wagons. This could be omitted when simulating short stop braking operations, in which only a small portion close to the wheel outer surface is subjected to a temperature rise, while the remaining part of the wheel is not affected by the application of the braking effort. Nonetheless, when modelling long-lasting drag braking operations, conduction inside the wheel can bring to a temperature rise even in regions that are far away from the contact zone, so that conduction towards the axle is not negligible. Therefore, to

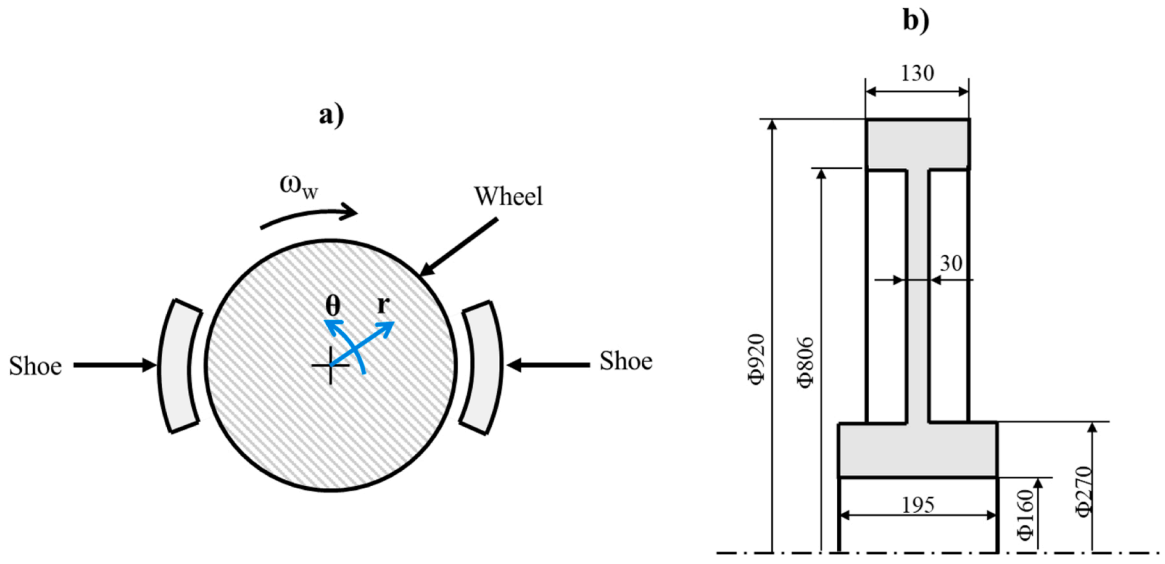

Fig. 2. Modelled wheel: a) 2Bg block configuration and b) Simplified wheel section geometry (dimensions in mm).

avoid building separate models for stop and drag braking operations, the models are developed with the previously described strategy to consider the thermal inertia of the axle.

It is important to highlight that the two models are mainly developed for transient analyses of typical tread braking operations, with the effect of wheel rotation modelled by defining the friction heat flux as a moving heat source, whilst keeping a fixed wheel mesh. However, at the initial stages of the model validation, steady-state analyses were launched to verify the grid discretization and to investigate the effect of the maximum order of retained harmonics on the simulation outputs.

Please note that the goal of the present paper is to validate the new 2D HAE-NAL model against the reference 3D Workbench model, proving that the same outputs can be obtained with a significant drop of the computational efforts. The experimental validation of the model is demanded to future activities, as the authors' research group has recently designed a new scaled twin-disc test bench [40] that will allow to carry out experimental tests considering different shoe materials and brake block configurations. The preliminary validation of the thermal models is going to be carried out with wheel rollers featuring a simplified shape, to avoid local differences caused by complex geometries.

2.1. Axisymmetric model with non-axisymmetric thermal loads

2.1.1. Mathematical description of the model

The 2D HAE-NAL model allows to calculate the temperature field in tread braked wheels considering the lack of axis symmetry of the thermal loads. In fact, for tread braking systems, the frictional heat flux produced at the wheel-shoe contact only acts on a limited circumferential portion of the wheel outer surface, thus violating the hypothesis of axisymmetric loads. Nonetheless, as the frictional heat flux entering the wheel still has a periodic trend along the wheel circumferential coordinate θ, with period of 2π, it can be approximated in the form of a Fourier transform series, as the sum of harmonic functions, as stated by Eq. (1):

$$\begin{gathered}\Phi_w(\vartheta) \approx \widetilde{\Phi}_w(\vartheta) = \sum_{h=0}^{N} \Phi_h^s \cos h\vartheta + \sum_{h=0}^{N} \Phi_h^a \sin h\vartheta = \sum_{h=0}^{N} \boldsymbol{\Theta_h}\boldsymbol{\Phi_h} \\ \boldsymbol{\Theta_h} = \left[\cos h\vartheta \quad \sin h\vartheta\right] \\ \boldsymbol{\Phi_h} = \left[\Phi_h^s \quad \Phi_h^a\right]^t\end{gathered} \tag{1}$$

where Φ_w is the frictional heat flux entering the wheel, $\widetilde{\Phi}_w$ is the corresponding Fourier series, N is the number of harmonic functions retained in the series, subscript h refers to the harmonic order and finally the terms Φ_h^s and Φ_h^a correspond to the harmonic amplitude coefficients for the cosine (symmetric) and sine (anti-symmetric) harmonic functions, respectively. The amplitude coefficients for the harmonic functions can be calculated according to Eq. (2):

$$\begin{cases} \Phi_0^s = \dfrac{1}{2\pi}\displaystyle\int_P \Phi_w(\vartheta)d\theta \\ \Phi_0^a = 0 \\ \Phi_h^s = \dfrac{1}{\pi}\displaystyle\int_P \Phi_w(\vartheta)\cos h\vartheta d\theta \quad h = 1 - N \\ \Phi_h^a = \dfrac{1}{\pi}\displaystyle\int_P \Phi_w(\vartheta)\sin h\vartheta d\theta \quad h = 1 - N \end{cases} \tag{2}$$

where $\int_P$ indicates integration over a period of the function, with common choices usually being intervals [0,2π] or [-π, π]. Please note that the Φ_0^s coefficient corresponds to the axisymmetric component of the thermal load, while the Φ_0^a coefficient is set to zero to keep the same summation counter for symmetric and anti-symmetric harmonics in Eq. (1).

The modelling approach adopted in this paper can be easily adopted for any distribution of the frictional heat flux along the circumferential direction, provided that the Fourier series coefficients are properly evaluated by means of Eq. (2), possibly needing numerical integration schemes for complex distributions evaluated from detailed wheel-shoe contact models [30]. For the sake of simplicity, this paper considers a constant heat flux on the wheel-shoe contact region, see Fig. 3, so the friction heat flux flowing into the wheel can be expressed as a function of the angular coordinate by means of Eq. (3):

$$\Phi_w(\vartheta) = \begin{cases} \Phi^*, \ \vartheta \le \dfrac{\vartheta_0}{2} \vee \vartheta \ge \left(2\pi - \dfrac{\vartheta_0}{2}\right) \\ \mathrm{H}(Bg)\Phi^*, \ \vartheta \ge \left(\pi - \dfrac{\vartheta_0}{2}\right) \wedge \vartheta \le \left(\pi + \dfrac{\vartheta_0}{2}\right) \\ 0, \ o.w. \end{cases} \tag{3}$$

where Φ^* is the flux entering the wheel at the contact with the shoe, ϑ_0 is the angular width of the wheel-shoe contact and finally H(Bg) is a function equal to 1 for 2Bg configuration and equal to 0 for 1Bg configuration, where a single shoe is pressed against the wheel outer surface. The average friction heat flux depends on the wheel-shoe pressing force and running speed, while the partitioning between wheel and shoes depends on their thermal properties and lateral surface. The interested reader can find further details on the calculation of the heat flux and partitioning factor in Appendix A. Please note that, although in this paper the hat flux is considered to be constant along the axial coordinate for all points belonging to the wheel tread, the method described below can be easily modified to consider the heat flux distribution coming from any bodies different from brake shoes with a constant width along the circumference.

Concerning the 2Bg block configuration, for which the H(Bg) function is unitary, the Fourier series amplitude values are as stated by the following Eq. (4):

$$\begin{cases} \Phi_0^s = \dfrac{\Phi^*\vartheta_0}{\pi} \\ \Phi_h^s = \dfrac{4\Phi^*}{h\pi}\sin\dfrac{h\vartheta_0}{2}\left|\cos\dfrac{h\pi}{2}\right| \quad \forall h \in [1, N] \\ \Phi_h^a = 0 \quad \forall h \in [0, N] \end{cases} \tag{4}$$

As expected, Eq. (4) states that only the symmetric harmonic functions (cosine functions) have non-zero coefficients, while all amplitude coefficients for the anti-symmetric components (sine functions) are equal to zero. Furthermore, the odd order harmonics have null coefficients, too, so that only terms Φ_0^s, Φ_2^s, Φ_4^s, etc. are useful contributions.

Regardless of the distribution of the heat flux over the contact region, once the Fourier series coefficients are determined, the temperature field is expressed in the same form as the thermal loads according to Eq. (5):

$$\begin{gathered}T(r, \vartheta, z) = \sum_{h=0}^{N} \mathrm{T}_h^s \cos h\vartheta + \sum_{h=0}^{N} \mathrm{T}_h^a \sin h\vartheta = \sum_{h=0}^{N} \boldsymbol{\Theta_h}\mathbf{T_h} \\ \mathbf{T_h} = \left[\mathrm{T}_h^s \quad \mathrm{T}_h^a\right]^t\end{gathered} \tag{5}$$

where T stands for temperature and superscripts a and s have the same meaning as in Eq. (1), thus referring to symmetric and anti-symmetric coefficients.

The calculation of the temperature field in the wheel can be obtained by writing the energy conservation principle over a finite computational domain V in variational form, as stated by Eq. (6) below:

$$\int_V \delta T \rho c \dot{T} dV + \int_V \nabla\delta T \bullet \boldsymbol{D} \nabla T dV = \int_{S2} \delta T \widetilde{\Phi}_w dS + \int_{S3} \delta T \alpha (T_B - T) dS \tag{6}$$

where δT is a virtual temperature change, $\int_V$ and $\int_S$ refer to integrals over finite volumes and finite surfaces, respectively, ρ is density, c is specific heat, **D** is the heat conductivity matrix, $\dot{T}$ is the temperature derivative, S_2 is the domain border where a prescribed heat flux is

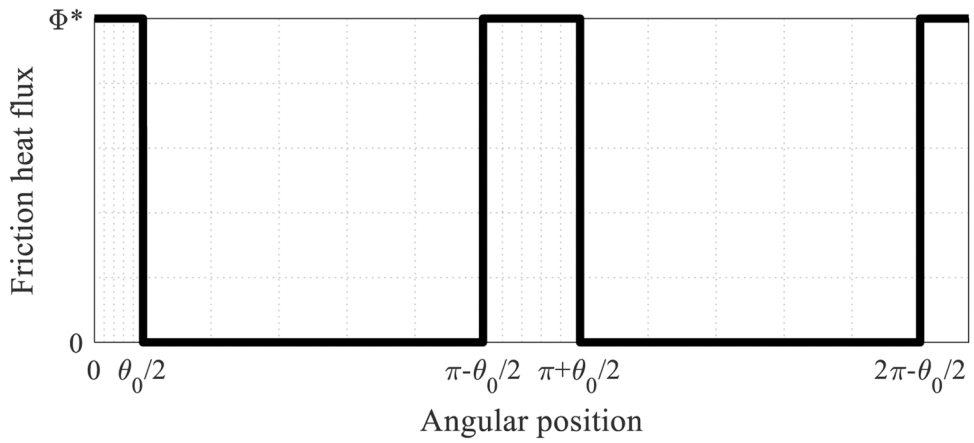

Fig. 3. Friction heat flux along the circumferential coordinate considered in this work.

applied and finally S_3 is a domain border where convection is prescribed, with a convection coefficient α and a bulk temperature of the surrounding fluid T_B. The finite computational domain corresponding to the wheel is divided into several finite elements, where temperature is assumed to vary in space according to pre-defined shape functions. For each harmonic order, the vector of harmonic amplitude coefficients $\boldsymbol{T_h}$ can be hence written as stated by Eq. (7):

$$\boldsymbol{T_h} = \boldsymbol{N}\boldsymbol{T_h^n} \tag{7}$$

where **N** is the shape function matrix and $\boldsymbol{T_h^n}$ is the vector of nodal temperatures, storing values for both symmetric and anti-symmetric functions. By combining Eq. (5) and Eq. (7), the temperature field and virtual temperature variations can be written as follows in Eq. (8):

$$\begin{aligned} T(r,\vartheta,z) &= \sum_{h=0}^{N} \boldsymbol{\Theta_h} \boldsymbol{N} \boldsymbol{T_h^n} \\ \delta T(r,\vartheta,z) &= \sum_{h=0}^{N} \boldsymbol{\Theta_h} \boldsymbol{N} \delta \boldsymbol{T_h^n} = \sum_{h=0}^{N} \delta \boldsymbol{T_h^{n\,t}} \boldsymbol{N^t} \boldsymbol{\Theta_h}^t \end{aligned} \tag{8}$$

Therefore, by including Eq. (8) and Eq. (1) into Eq. (6), the energy conservation principle over the finite domain is stated by the following Eq. (9):

$$\begin{aligned} \boldsymbol{M}\dot{\boldsymbol{T}}^{\boldsymbol{n}} + \boldsymbol{K}\boldsymbol{T}^{\boldsymbol{n}} &= \boldsymbol{Q_\Phi} + \boldsymbol{Q_\alpha} \\ \boldsymbol{K} &= \boldsymbol{K_D} + \boldsymbol{K_\alpha} \end{aligned} \tag{9}$$

where $\boldsymbol{T^n}$ is the vector of nodal temperatures for all harmonic orders and functions, $\dot{\boldsymbol{T}}^{\boldsymbol{n}}$ is its time derivative, **M** is the specific heat matrix, **K** is the system stiffness matrix, i.e., the sum of the heat conductivity matrix $\mathbf{K_D}$ and the matrix accounting for the contribution given by convection $\mathbf{K_\alpha}$, and finally $\boldsymbol{Q_\Phi}$ and $\boldsymbol{Q_\alpha}$ are the vector of applied heat fluxes and convection vector for all orders and symmetry types. The terms introduced in Eq. (9) can be defined by comparison with Eq. (6), see the following Eq. (10):

$$\begin{aligned} \boldsymbol{M} &= \sum_{h=0}^{N}\sum_{l=0}^{N} \int_V \boldsymbol{N^t}\boldsymbol{\Theta_h}^t \rho c \boldsymbol{\Theta_l} \boldsymbol{N} dV = \sum_{h=0}^{N}\sum_{l=0}^{N} \boldsymbol{M_{hl}} \\ \boldsymbol{K_D} &= \sum_{h=0}^{N}\sum_{l=0}^{N} \int_V \nabla(\boldsymbol{N^t}\boldsymbol{\Theta_h}^t) \bullet \boldsymbol{D} \nabla(\boldsymbol{\Theta_l}\boldsymbol{N}) dV = \sum_{h=0}^{N}\sum_{l=0}^{N} \boldsymbol{K_{D,hl}} \\ \boldsymbol{K_\alpha} &= \sum_{h=0}^{N}\sum_{l=0}^{N} \int_{S3} \alpha \boldsymbol{N^t}\boldsymbol{\Theta_h}^t \boldsymbol{\Theta_l} \boldsymbol{N} dS = \sum_{h=0}^{N}\sum_{l=0}^{N} \boldsymbol{K_{\alpha,hl}} \\ \boldsymbol{Q_\Phi} &= \sum_{h=0}^{N} \int_{S2} \boldsymbol{N^t}\boldsymbol{\Theta_h}^t \boldsymbol{\Theta_h} \boldsymbol{\Phi_h} dS \\ \boldsymbol{Q_\alpha} &= \sum_{h=0}^{N} \int_{S3} \alpha T_B \boldsymbol{N^t}\boldsymbol{\Theta_h}^t dS \end{aligned} \tag{10}$$

Focusing on the specific heat and thermal conductivity matrixes, assuming constant material properties, as the infinitesimal volume can be expressed in cylindrical coordinates as $dV = rdrd\vartheta dz$, and since the only terms depending on the angular coordinate are those stored in the $\boldsymbol{\Theta_h}$ matrixes, it can be proved that the above expressions always include the integrals in Eq. (11) below, whose solution is known a priori in view of the orthogonality properties of the sine and cosine functions:

$$\begin{aligned} \int_P \cos h\vartheta \sin l\vartheta d\theta &= 0 \forall h,l \\ \int_P \cos h\vartheta \cos l\vartheta d\theta &= \begin{cases} 0, h \neq l \\ 2\pi, \quad h = l = 0 \\ \pi, h = l \neq 0 \end{cases} \\ \int_P \sin h\vartheta \sin l\vartheta d\theta &= \begin{cases} 0, h \neq l \\ 0, \quad h = l = 0 \\ \pi, h = l \neq 0 \end{cases} \end{aligned} \tag{11}$$

Therefore, the orthogonality property proves that all integrals due to the product of different harmonic types or orders are always zero. This means that the specific heat and thermal stiffness matrix of the system can be written as stated by Eq. (12):

$$\begin{aligned} \boldsymbol{M} &= \mathrm{diag}\left(\boldsymbol{M_{00}^s}, \boldsymbol{M_{00}^a}, \ldots, \boldsymbol{M_{hh}^s}, \boldsymbol{M_{hh}^a}, \ldots, \boldsymbol{M_{NN}^s}, \boldsymbol{M_{NN}^a}\right) \\ \boldsymbol{K} &= \mathrm{diag}\left(\boldsymbol{K_{00}^s}, \boldsymbol{K_{00}^a}, \ldots, \boldsymbol{K_{hh}^s}, \boldsymbol{K_{hh}^a}, \ldots, \boldsymbol{K_{NN}^s}, \boldsymbol{K_{NN}^a}\right) \end{aligned} \tag{12}$$

hence proving that the solution can be obtained by independently solving N_{eff} independent problems, with N_{eff} being the number of non-zero coefficients in the Fourier series of the thermal flux, see Eq. (1). This is the biggest benefit of the adopted approach, since a 2D HAE-NAL model includes a lower number of nodes with respect to an equivalent 3D model, and the solution can be obtained by taking advantage of

parallel computing, because the contribution given by each harmonic can be solved independently. This means that the new 2D HAE-NAL model can potentially provide the desired outputs at the same computational cost of traditional pure axisymmetric models, provided that proper distributed/parallel computing techniques are deployed. Furthermore, the new 2D HAE-NAL model can be extended to consider the dependency of material parameters on temperature at a small computational cost. This can be done by launching a preliminary standalone FE simulation for the 0-th order harmonic to obtain the average circumferential temperature in all radial and axial positions. The simulations for all other harmonics can then be launched considering the thermal properties evaluated at the average temperature. Potentially, the computational cost is only doubled with respect to a pure axisymmetric simulation, as all simulations for harmonic orders different from zero can run in parallel after the preliminary simulation for the 0-th order component.

2.1.2. Model implementation

At this stage of the activity, the new 2D HAE-NAL model, sketched in Fig. 4a), is implemented in the ANSYS Mechanical APDL code, meshing the wheel section with the PLANE78 element type, featuring eight nodes with a single DOF, i.e., the node temperature, and cubic shape functions. Since the temperature field along the circumferential direction can be obtained by solving a separate independent problem for each harmonic contribution, as proved in the previous subsection, the ANSYS PLANE78 element type has shape functions that change based on the considered harmonic order and function [43,44]. The latter can be specified using the ANSYS MODE command, that allows to define the desired harmonic function (symmetric or anti-symmetric) and order. Therefore, the shape functions for the selected harmonic contribution in natural coordinates are expressed as stated by Eqs. (13) and (14):

$$\boldsymbol{N}_{78,h}^{m} = \boldsymbol{N}_{axsym}(\xi,\eta) \bullet f_h^m(\vartheta) \qquad m = s,a \tag{13}$$

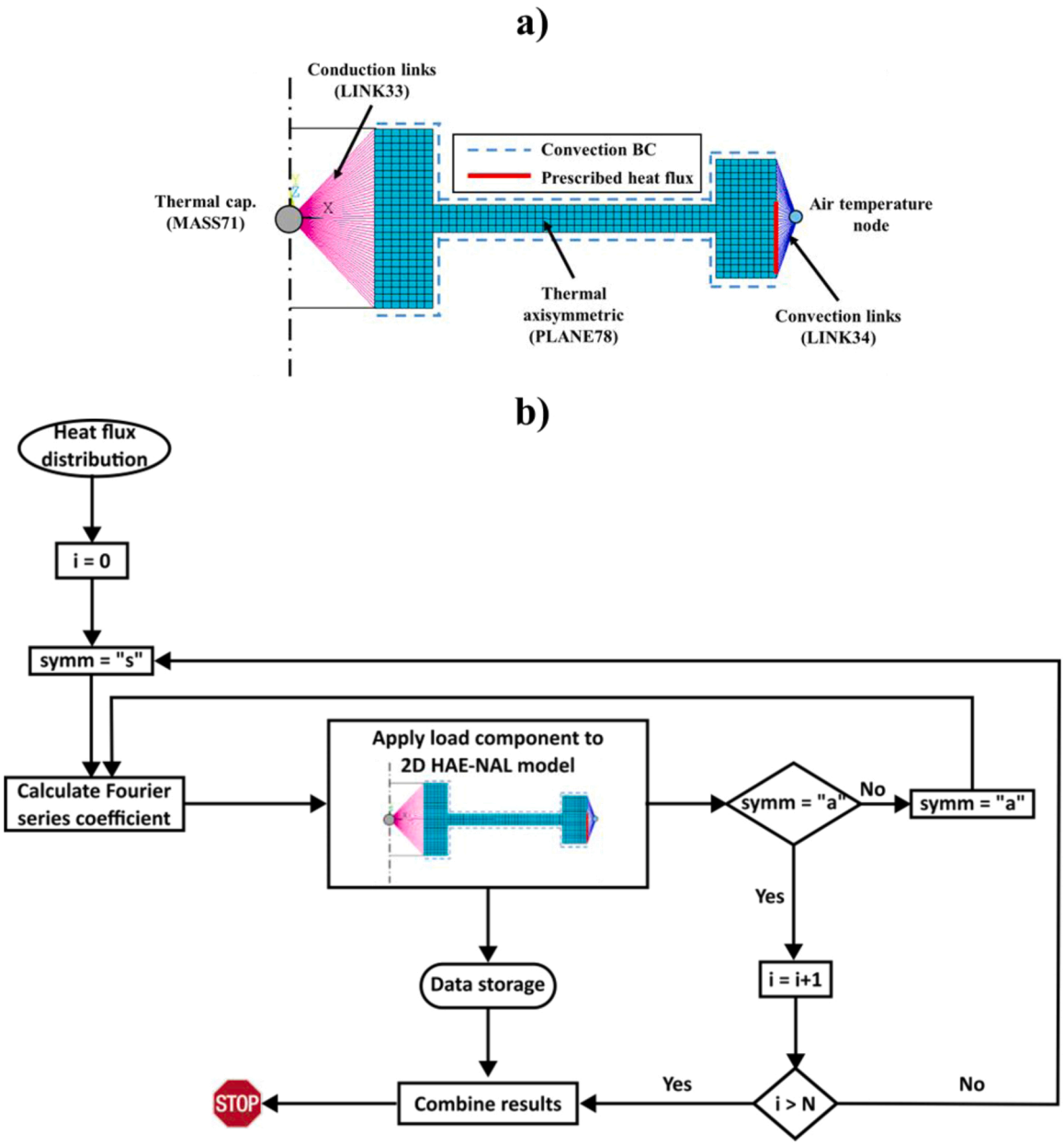

Fig. 4. 2D HAE-NAL model implementation: a) ANYSYS APDL model elements and BCs and b) Flow-chart of the simulations.

$$f_h^m(\vartheta) = \begin{cases} \cos h\vartheta, & m = s \\ \sin h\vartheta, & m = a \end{cases} \tag{14}$$

where $\boldsymbol{N}_{78,h}^{m}$ is the shape stiffness matrix of the PLANE78 element for the h-th harmonic order and symmetry type identified by superscript m ("s" for symmetric or "a" for anti-symmetric), ξ and η are the natural coordinates along radial and axial direction (please note that they are identified as s and t in ANSYS documentation [44]) and finally $\boldsymbol{N}_{axsym}(\xi,\ \eta)$ is a matrix that describes the dependency of shape functions over axial and radial coordinates. This matrix does not depend on the considered harmonic order, and for a quadrilateral element it is identical to shape functions used for traditional purely axisymmetric elements, as stated by Eq. (15):

$$\boldsymbol{N}_{axsym}(\xi,\eta) = \begin{bmatrix} \frac{1}{4}(1-\xi)(1-\eta)(-\xi-\eta-1) \\ \frac{1}{4}(1+\xi)(1-\eta)(\xi-\eta-1) \\ \frac{1}{4}(1+\xi)(1+\eta)(\xi+\eta-1) \\ \frac{1}{4}(1-\xi)(1+\eta)(-\xi+\eta-1) \\ \frac{1}{2}(1-\xi^2)(1-\eta) \\ \frac{1}{2}(1+\xi)(1-\eta^2) \\ \frac{1}{2}(1-\xi^2)(1+\eta) \\ \frac{1}{2}(1-\xi)(1-\eta^2) \end{bmatrix}^t \tag{15}$$

With the ANSYS PLANE78 element, the heat flux coefficients for each harmonic contribution are specified by properly setting the MODE command, so that the nodal temperatures can be calculated independently for each harmonic order and symmetry type. One of the greatest challenges in the model is the need for considering the rotation of the wheel with respect to the brake blocks. In fact, as the wheel rotates with the brake shoes pushed against the tread, the circumferential sectors of the wheel subjected to the frictional heat flux change with time. This is a modelling challenge that is faced in the analysis of other types of braking systems such as disk brakes, as well. Recently, for disk brake applications, different types of mathematical functions, including first-order sinusoidal [45] and Gaussian [46] functions, were tested to consider the relative rotation effect. These functions are used to approximate the time history of the heat flux without considering a uniform heat flux value across the whole circumference, whilst still preventing from the implementation of complex strategies to prescribe BCs varying with both space and time. Although valuable, this method is simplified, hence the new 2D HAE-NAL model reproduces rotation with a well-established approach in the literature, that considers the point of view of an observer that moves with the wheel [30,47,48]. With this approach, the wheel (or disc in disc brake systems) is fixed, and the thermal load changes in time. However, whilst implementing this approach in 3D models is quite straightforward, considering the heat flux rotation in the 2D HAE-NAL model is more complex. In fact, for the 2D HAE-NAL model, the heat flux rotation must be applied for each separate harmonic order contribution. For a selected harmonic order and symmetry type, the heat flux coefficient after rotation depends on both symmetric and anti-symmetric Fourier series terms. Precisely, the new heat flux coefficients after a rotation from a reference initial position can be obtained according to the following Eq. (16):

$$\begin{aligned} \boldsymbol{\Phi_h}' &= \boldsymbol{R_h}\boldsymbol{\Phi_h} \\ \boldsymbol{\Phi_h}' &= \begin{bmatrix} \Phi_h^{s\prime} & \Phi_h^{a\prime} \end{bmatrix}^t \\ \boldsymbol{R_h} &= \begin{bmatrix} \cos h\Delta\vartheta & \sin h\Delta\vartheta \\ -\sin h\Delta\vartheta & \cos h\Delta\vartheta \end{bmatrix} \end{aligned} \tag{16}$$

where the apostrophe is used to indicate the coefficients corresponding to a relative rotation Δθ and $\mathbf{R_h}$ is the rotation matrix for harmonic functions of the h-th order.

To practically implement Eq. (16) above in the 2D HAE-NAL model, ANSYS table data type variables are specifically defined in the APDL routine in the pre-processing stage. ANSYS tables are specific variable types that can be used to define loads varying with both space and time. The heat flux Fourier series coefficients are linearly proportional to the average value of heat flux acting at the wheel-shoe contact interface, as stated by Eq. (4). Therefore, as the applied heat flux can change with time, it is possible to simply obtain the Fourier series coefficients for a unitary flux and then scale these values by the considered heat flux value. Furthermore, to account for the rotation of the heat flux with respect to the wheel, it is not required to solve the integrals defined in Eq. (2) at each time-step, as it is possible to only calculate the Fourier series coefficients for a reference position and then apply the transformation in Eq. (16). Based on these considerations, in the ANSYS APDL routine, a table variable is defined to store the time-history of the heat flux, namely the values of the function $\Phi^*(t)$ at discrete time-steps. Moreover, for a specific harmonic order, the symmetric and anti-symmetric Fourier series coefficients obtained for a reference initial position are loaded and stored as scalar variables. The reference initial position of the blocks with respect to the wheel is the one corresponding to the distribution in Fig. 3. Prior to the solution of the 2D HAE-NAL model, a table with the values of heat flux coefficients to be applied for the considered harmonic order and function is filled in a "for" loop by implementing the following Eq. (17):

$$\begin{cases} \Phi_h^{s\prime}(t) = \Phi^*(t) \bullet \left\{ \Phi_{h,unit}^{s} \cos[h\Delta\vartheta(t)] + \Phi_{h,unit}^{a} \sin[h\Delta\vartheta(t)] \right\} \\ \Phi_h^{a\prime}(t) = \Phi^*(t) \bullet \left\{ -\Phi_{h,unit}^{s} \sin[h\Delta\vartheta(t)] + \Phi_{h,unit}^{a} \cos[h\Delta\vartheta(t)] \right\} \end{cases} \tag{17}$$

where $\Phi_{h,unit}^{s}$ and $\Phi_{h,unit}^{a}$ are the Fourier series coefficients calculated for a unitary heat flux and for the reference initial position, while $\Delta\vartheta(t)$ is the rotation with respect to the reference position for each time-step, which is stored in a separate table data type variable and can be obtained from either simulations, as done in this paper, or experimental data. Please note that for the 2Bg brake block configuration considered in this work, the coefficients $\Phi_{h,unit}^{a}$ are all equal to zero, thus meaning that Eq. (17) simplifies as stated by Eq. (18).

$$\begin{cases} \Phi_h^{s\prime}(t) = \Phi^*(t) \bullet \Phi_{h,unit}^{s} \cos[h\Delta\vartheta(t)] \\ \Phi_h^{a\prime}(t) = -\Phi^*(t) \bullet \Phi_{h,unit}^{s} \sin[h\Delta\vartheta(t)] \end{cases} \tag{18}$$

Nonetheless, it is worth mentioning that, although for the reference position the anti-symmetric coefficients of the Fourier series are all zeros, the anti-symmetric coefficients after rotation are different from zero, so that their contribution must be considered when solving the model.

The outer surface of the wheel is subjected to both frictional heat flux in the tread region and convection. The heat flux is directly applied on the mesh nodes belonging to the wheel tread as BC. Precisely, as brake blocks typically feature an axial with of 80 mm, the heat flux is applied on nodes with axial coordinates in the range −55 mm to + 25 mm. The nodes subjected to heat flux are also subjected to convection with the ambient air, however ANSYS does not allow to directly prescribe two different types of BC on the same elements and nodes. To tackle this limitation, the effect of convection on the outer surface is modelled through the introduction of uniaxial convection link elements (LINK34 in ANSYS), which connect all nodes of the outer surface to an external

node kept to a constant temperature value, corresponding to the ambient air temperature. A similar strategy is adopted for the inner surface of the wheel, which is directly mounted on the wheel axle. All nodes belonging to the inner surface are connected to a central element with lumped thermal capacitance (MASS71 element in ANSYS) by means of conduction links (ANSYS LINK33 element type). The thermal capacitance prescribed on the central element is calculated equal to the thermal capacitance of half the axle. Finally, on the remaining surfaces, a convection boundary condition is prescribed. As previously, stated, the model currently does not consider thermal radiation, whose contribution is surely less important than those of friction heat flux and air convection in the temperature range reached during tread braking service operations. Although the ANSYS PLANE78 element type formally does not allow the direct application of radiation loads, the model could be enhanced in the future to account for the effect of radiation loads with a simplified approach, i.e., by adding radiation link elements (ANSYS LINK31 element type) only for the 0-th order harmonic, i.e., the purely axisymmetric contribution, thus considering the "average" radiation contribution.

Since the 2D HAE-NAL model is currently implemented based on elements directly available in the ANSYS package, its modelling capabilities are affected by the limitations of the PLANE78 element type, namely, i) the need for a linear material behaviour, ii) the incapability of directly applying radiation loads and iii) the application of loads that can be approximated as a sum of harmonic contributions of different orders [44]. Whilst the last limitation cannot be overcome, as the method on which the 2D HAE-NAL model relies on is specifically suited for periodical loads that can be approximated with Fourier series, the first and second limitations can be partially mitigated. In fact, as already explained above, it could be possible to consider the "average" effect of radiation, by applying radiation links on the pure harmonic contribution only (0-th order harmonic).

A similar strategy could be implemented to consider the thermal dependency of material properties on temperature. At the current state of the model development, simulations are run considering constant thermal properties for the wheel, which are extracted from the typical range given in reference [25] and listed in Table 1. Nonetheless, in future works, the dependency of the wheel steel properties on temperature can be included with an average approach, i.e., by adopting the thermal properties at the temperature values obtained from a standalone simulation run for the axisymmetric mode (order zero and cosine function).

Fig. 4b) shows the flow-chart implemented to run the simulations for the different harmonic orders and symmetry types (cosine or sine). The major input for the simulations is the heat flux distribution, for which the Fourier series coefficients are calculated with a MATLAB script. The same MATLAB script is used to start ANSYS APDL sessions for the model setup with application of BCs for all retained harmonics in the Fourier series. In view of the properties of the 2D HAE-NAL model described above, the loops in the flow-chart are not sequential, as they can be run in parallel by calling separate sessions at the same time from batch. The results of each ANSYS APDL session are then combined at the end of the simulations. At this early stage of the activity, the model does not explicitly take advantage of parallel computing, however the solution for the different harmonic modes is obtained by running multiple ANSYS sessions at the same time from a batch script.

Please note that, whilst relying on element types available in commercial codes simplifies the model setup, to the authors' knowledge, the application of harmonic axisymmetric elements for the investigation of the temperature field in tread braked wheels is a novelty in the field. Furthermore, the practical implementation of the flow-chart in Fig. 4b) is not trivial, as there exist several modelling challenges to be faced and solved, such as managing the rotation of the heat flux, considering its variations in time and along the circumferential direction and effectively combining the outputs obtained for the different harmonic orders. While details on the former point are given in the lines above, the combination of the different harmonic contributions is done with a MATLAB script that loads files saved at the end of the simulation for each considered harmonic order and symmetry type. The files store the nodal temperature results, which correspond to Fourier series coefficients of temperatures for the considered harmonic orders and functions. Therefore, the Fourier series coefficients for temperature are easily combined in MATLAB to generate the temperature time history for different circumferential positions. The MATLAB script combining the outputs obtained for each harmonic contribution was validated against the ANSYS built-in LCOPER function in steady-state simulations.

Moreover, although in this paper the 2D HAE-NAL model is built using element types already available in the ANSYS library, the method shown in the previous subsection could be implemented within any in-house code, provided that the mathematical formalism is correctly applied. This is going to be faced by the authors in future activities, where the approach will be further simplified to obtain a 1D axisymmetric model that has enough computational efficiency to be solved by the same numerical integrator used for the vehicle dynamics simulation in MB codes. For this purpose, the model will be implemented as an in-house FORTRAN routine and compiled into a.dll file.

Table 1
Main properties of the wheel steel adopted in the model.

Quantity	Symbol	Value	Unit
Density	ρ	7818	kg/m^3
Specific Heat	c	487	J/(kg·K)
Thermal conductivity	λ	50	W/(m·K)

2.2. 3D model

The 3D model of the tread braked wheel is implemented within the ANSYS Workbench software package, see Fig. 5. In view of its higher complexity level, the 3D model serves as the benchmark for the new 2D HAE-NAL model. The mesh of the 3D geometry is obtained as the revolution of the mesh of the wheel section developed for the 2D HAE-NAL model, using the PULL function available in ANSYS Workbench. The final mesh is made with SOLID279 thermal elements, with 20 nodes and quadratic shape functions. Convection is applied on the same surfaces as for the 2D HAE-NAL model, with no need for the implementation of the strategy based on convection link elements. In fact, for 3D models, Workbench defines layers of SURF152 elements, which are superimposed over solid elements for the prescription of different kinds of BCs. The prescription of the rotating friction heat flux is obtained with a user routine implementing APDL commands. The user routine defines an additional layer of SURF152 elements added over the wheel tread surface, and the heat flux on the layer is provided as a function of time and angular position by means of a table data type variable. The table is

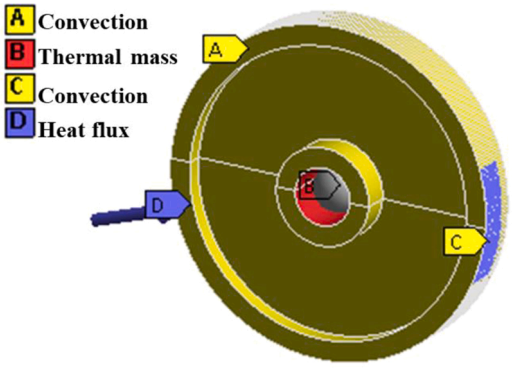

Fig. 5. 3D model in ANSYS Workbench with BCs (heat flux rotates during the simulation).

loaded from a.csv file generated with a MATLAB script, that builds a matrix implementing the periodic shift of a rectangular Boolean function whose value is equal to 1 in the regions that are in contact with the block and zeros elsewhere. The matrix, filled with Boolean values, is then multiplied by the time history of the average heat flux at the wheel-shoe contact interface, that is calculated as described in Appendix A and Appendix B. This approach is similar to the one suggested by Grzes [48] for a disc brake system, although for tread braked systems the dependency of the heat flux on the radial coordinate can be disregarded, due to the small variation of radius along the axial direction in the tread region. Therefore, the table generated to manage the application of the rotating heat flux is a 2D matrix, that accounts for the dependency of the heat flux on angular coordinate and time. The spatial dependency on the angular coordinate reflects the relative rotation between the wheel and brake blocks, while the time dependency accounts for the variation of the dissipated power with time. In fact, in the case of transient stop braking operations, the braking effort changes with time, due to the time needed to fill the brake cylinders, whilst at the same time speed decreases, see again Appendix A and Appendix B.

The connection of the inner surface nodes to the central thermal capacitance mass representing half of the axle is managed by the ANSYS Workbench package through the automatic definition of ANSYS special contact elements, namely a layer of CONTA174 elements on the inner surface nodes paired with a TARGE170 element attached to the thermal capacitance mass node.

3. Results

This section shows the results of the simulations run to prove the modelling capabilities of the new 2D HAE-NAL model. Table 2 summarizes the simulations shown in the following subsections and the goals of each analysis. It can be observed that the complexity level of the simulated scenario increases from simulation 1–3. Simulation 1 is carried out to verify the grid discretization, so it only considers the purely axisymmetric contribution (0-th order harmonic). Furthermore, simulation 1 is run specifically to prove that, at least when an axisymmetric heat flux is considered, the 2D HAE-NAL model provides the same outputs as the 3D reference model. Simulation 2 is still a steady-state simulation, but the heat flux is applied only in the tread region where the wheel contacts with the shoes in the reference initial position, see Fig. 5. Although the new 2D HAE-NAL model can consider the rotation of the wheel by applying the friction heat flux BC as a moving heat source in transient simulations, this preliminary steady-state analysis is run considering a fixed heat flux. Therefore, the results are not representative of the real thermal behaviour of tread braked wheels. Although it does not have a physical meaning, and huge temperature values are calculated, simulation scenario 2 is selected to prove the validity of the 2D HAE-NAL model in conditions where the temperature varies along the circumferential direction and to estimate the maximum harmonic order that should be retained in the Fourier series. Finally, the scenario with the highest level of complexity is the one addressed by simulation 3, that involves a transient analysis of a stop braking simulation considering a non-axisymmetric and moving heat flux. Therefore, this simulation allows to prove the validity of the 2D HAE-NAL model under conditions of transient braking operations considering the relative rotation between the wheel and the brake blocks.

Table 2
Simulations run to assess and prove the capabilities of the 2D HAE-NAL model.

No. Simulation	Analysis type (Operation)	Heat flux distribution	Goals
1	Steady-state (Drag braking)	Axisymmetric	Verify mesh grid discretization. Validate the 2D HAE-NAL model under pure axisymmetric conditions
2	Steady-state (Drag Braking)	Non-axisymmetric, fixed	Validate the 2D HAE-NAL model under conditions of non-axisymmetric loads. Identify the number of harmonic orders to be retained in the Fourier series
3	Transient (Stop braking)	Non-axisymmetric, moving	Validate the 2D HAE-NAL model under transient scenarios with moving load.

For all simulations the ambient air temperature is set to 20°C, while the convection coefficient is estimated from literature correlations [25] and set equal to 60 W/(m^2·K), that is in the typical range for forced convection. The convection coefficient is applied as a constant value on all free surfaces. In fact, despite being a function of radial position and peripheral speed, since it is usually extracted from experimental correlations of the Prandtl and Reynolds' numbers, the convection coefficient is the model parameter with the highest uncertainty. As the primary goal of this paper is to prove that the 2D HAE-NAL produces the same outputs as the reference 3D model, it is believed that this simplifying assumption does not compromise the validity of the described activity. In future developments, the authors are planning to perform experimental tests on scaled twin-disc devices, and the collected data will be used to tune the convection coefficient to be applied in the model, considering its dependency on speed and radial coordinate.

3.1. Mesh discretization tests

The analysis labelled as simulation 1 in Table 2 is initially run to perform a mesh discretization test on the 2D HAE-NAL model to identify the optimal mesh grid size on the elements on the outer surface, where the frictional thermal flux is applied, and a steep thermal gradient is expected. To speed up the simulation times, the mesh discretization test is carried out on a steady-state simulation scenario, considering the results for the 0-th order harmonics only. The results for steady-state simulations with the application of a constant flux can be considered as the limit temperature field of long-lasting drag braking operations. In such conditions, it can be assumed that the temperature field is uniform along the circumferential direction, and the temperature field is indeed axisymmetric. The reference value of uniform heat flux applied in the mesh grid discretization is equal to 160189 W/m^2, that coincides with an average heat flux value of 720849 W/ m^2 at the contact between each shoe and the wheel tread in a 2Bg configuration. This value is calculated as the heat flux flowing into the wheel at the wheel-shoe contact for P10 cast iron shoes when a 22.5-ton axle-load wagon runs on a downhill track section with slope of 21 ‰ at constant speed of 70 km/h, i.e., the reference drag braking operation defined by the European regulation [49], which is commonly known as the "TSI Wag". Further details on the calculation of the heat flux can be found in Appendix A and Appendix B.

The mesh on the wheel cross-section of the 2D HAE-NAL model is generated and controlled through the definition of a dedicated variable that allows to change the number of elements along the outer wheel surface. As the present paper is mainly focused on validating the 2D HAE-NAL APDL model against the reference 3D Workbench model, a regular mesh pattern is generated to avoid excessive distortion in the elements, see Fig. 4. This makes it easier to obtain the same mesh pattern in the two models, thus avoiding numerical discrepancies that could compromise the comparison of the developed models. The convergence of the mesh grid is assessed in terms of the temperature measured on the wheel outer surface on two nodes, namely one node in the middle of the wheel (axial coordinate equal to zero) and one node in the middle of the tread (axial coordinate equal to −15 mm), where the largest temperature is expected. Furthermore, the average temperature of all nodes on the outer surface belonging to the tread is assessed. The results of the mesh grid discretization test are shown in Fig. 6, where the temperature values on the two nodes and the average tread temperature are plotted as a function of the number of elements on the outer surface. It is found

from the mesh grid discretization tests that a good convergence can be obtained if the wheel outer surface is discretized with 31 elements or more.

Please note that the optimal wheel mesh identified from the simulations shown in this subsection is used in the 3D model built in ANSYS Workbench, too, since the 3D mesh is generated as the revolution of the mesh of a cross-section through the PULL function available in Workbench.

3.2. Validation

This subsection specifically addresses the main goal of the paper, namely the validation of the 2D HAE-NAL model implemented in ANSYS Mechanical APDL against the reference 3D model built in the ANSYS Workbench environment, which is considered as the benchmark due to its higher complexity. The benchmarking against the reference 3D model is carried out under different simulation scenarios with increasing levels of complexity as shown in Table 2.

3.2.1. Steady-state analysis with purely axisymmetric heat flux

A preliminary validation, aiming to compare the outputs of the 2D HAE-NAL model against those calculated with the reference 3D model, is performed on the same scenario used for mesh grid discretization test purposes, namely simulation 1 shown in Table 2. The good agreement between the two models is highlighted in Fig. 7, which shows the temperature field on a wheel cross-section calculated with the 2D HAE-NAL model and Workbench 3D model when applying the reference uniform heat flux equal to 160189 W/m^2 along the wheel circumferential direction. Therefore, it is proved that the 2D HAE-NAL model gives the same results as the reference 3D model in a steady-state analysis under the application of purely axisymmetric thermal loads.

3.2.2. Steady-state analysis with fixed non-axisymmetric heat flux

After proving the basic capabilities of the 2D HAE-NAL model when dealing with pure axisymmetric loads in a steady-state analysis, a further validation is carried out under the conditions of simulation scenario 2, see Table 2. As for simulation 1, simulation 2 is still a steady-state analysis, but in this case, the heat flux is non-uniform along the circumferential direction, as it is applied as a fixed thermal load acting only on a limited circumferential portion of the tread. In the 3D Workbench model, the heat flux applied at each contact patch with the shoe is 720849 W/m^2, thus considering the same reference drag braking operation as for the mesh discretization test shown in the lines above. For the 2D HAE-NAL model, different simulations are run increasing the number of retained harmonics, to assess the influence of the maximum considered harmonic order on the results.

Fig. 8 shows the temperature variation along the circumferential direction for the node in the middle of the wheel outer surface (axial coordinate equal to 0), with a zoom on the temperature peak occurring at circumferential positions around the 180° location. Results are given for the 3D Workbench model, where the "exact" flux is applied on a limited portion of the wheel circumference, as well as for simulations with the 2D HAE-NAL model run with increasing maximum order of retained harmonics in the Fourier series (5-th, 10-th, 15-th, 20-th, 30-th and 40-th orders are plotted). The results of the 2D HAE-NAL model overlap the outputs of the 3D model when the maximum considered harmonic order is at least equal to 15. Therefore, the capability of the 2D HAE-NAL model of predicting the temperature variation along the wheel circumference with values that are consistent with the 3D model is proved.

3.2.3. Transient analysis with moving non-axisymmetric heat flux

After benchmarking the 2D HAE-NAL model against the reference 3D model in steady-state simulations, considering both axisymmetric and non-axisymmetric heat flux applications, the capabilities of the new model are demonstrated in a transient analysis of a reference stop braking operation. This scenario, corresponding to simulation 3 in Table 2, considers a moving non-axisymmetric heat flux, that varies with time. The reference stop braking operation is selected as the emergency braking operation of a 20-ton axle-load freight wagon equipped with a pneumatic empty-loaded device as defined in Appendix O of the UIC 544–1 leaflet [50].

The inputs for the thermal FE models are calculated from the longitudinal dynamics (LTD) of the isolated braked freight wagon. The LTD is simulated with a simplified approach based on a heuristic exponential law for the pressure rise in the brake cylinder [51], see Appendix B for additional details. The LTD simulation, run through a separated MATLAB code implementing functions used in the LTDPoliTo code developed by the research group in past activities [52–54], allows to estimate the braking forces and the speed profile during the braking operation, thus providing the quantities needed for the calculation of the average heat flux flowing into the wheel. The interested reader can find further information on the implemented routine for the simulation of the LTD of the isolated vehicle in [30] and in Annex B.

Fig. 9 shows the time histories of the main quantities of interest calculated from the LTD simulation, which are then fed to the FE

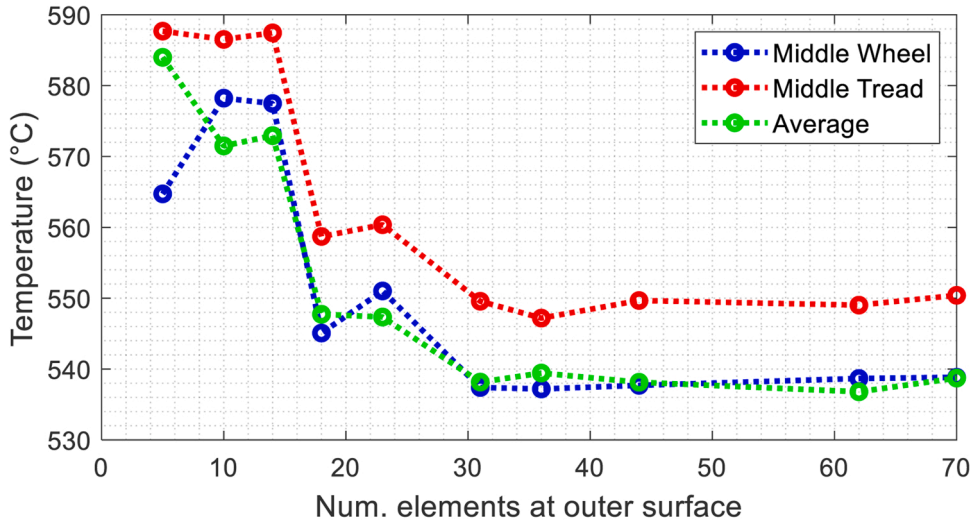

Fig. 6. Mesh grid discretization test for the 2D model built in ANSYS APDL.

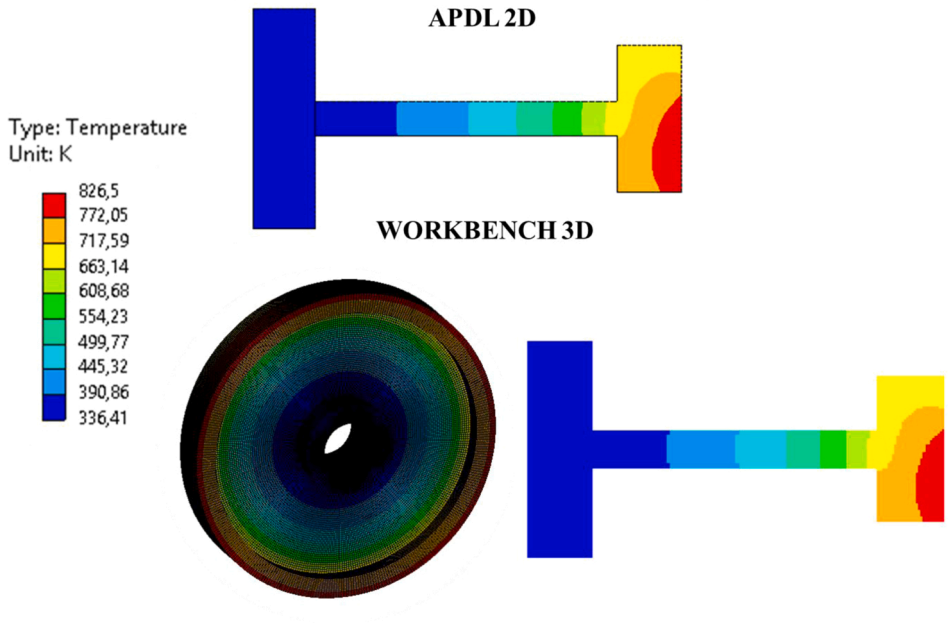

Fig. 7. Results of the two models for the reference steady-state simulation considering uniform heat flux along the wheel circumference (simulation 1).

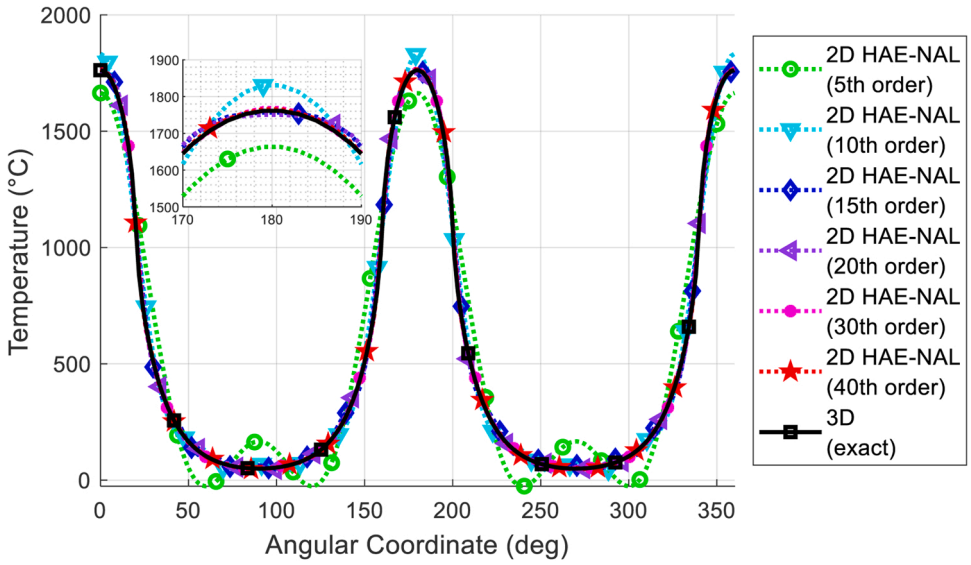

Fig. 8. Benchmarking of the 2D HAE-NAL model against the 3D model in a steady-state operation for increasing maximum order of retained harmonics.

thermal models. Precisely, Fig. 9a) illustrates the speed profile until standstill, Fig. 9b) provides the time evolution of the brake shoe pressing force and finally Fig. 9c) shows the variation of the heat flux flowing into the wheel during the stop braking operation. It can be noticed from Fig. 9c) that the heat flux has a non-monotonic trend, since it is proportional to both braking force and speed. In fact, at the beginning of the stop braking operation, the braking force is low while speed is high, and the flux rises. After filling the brake cylinder and saturating the wheel-shoe normal contact force, the vehicle decelerates and the heat flux decreases, accordingly. Furthermore, Fig. 9a) shows that speed has a nonlinear trend with time, and this is mainly due to the modelling of the wheel-shoe friction coefficient, which is dependent on the pressing force and speed, see Appendix B. Therefore, even after saturating that brake cylinder pressure, as speed decreases during the stop braking operation, the friction coefficient tends to increase, so that with the same wheel-shoe pressing force, the braking force increases as well, thus generating a higher deceleration.

Please note that although speed decreases during the stop braking operation, which would reduce the convection coefficient, the preliminary simulations in this paper are run with the constant value of the convection coefficient of 60 W/(m^2·K), since the major goal of the activity is to demonstrate the capabilities of the 2D HAE-NAL model. However, the model can be easily upgraded in the future to account for the dependency of the convection coefficient on speed and radial position, based on experimental data that will be collected from scaled test rigs which are being specifically designed by the authors' research group. The main model inputs for the transient simulation of the reference stop braking operation are given in Table 3.

Fig. 10 shows the time history of the temperature of the node on the outer surface in the middle of the tread (axial coordinate equal to −15 mm) during the reference stop braking operation calculated with the two models, together with the output obtained from a purely

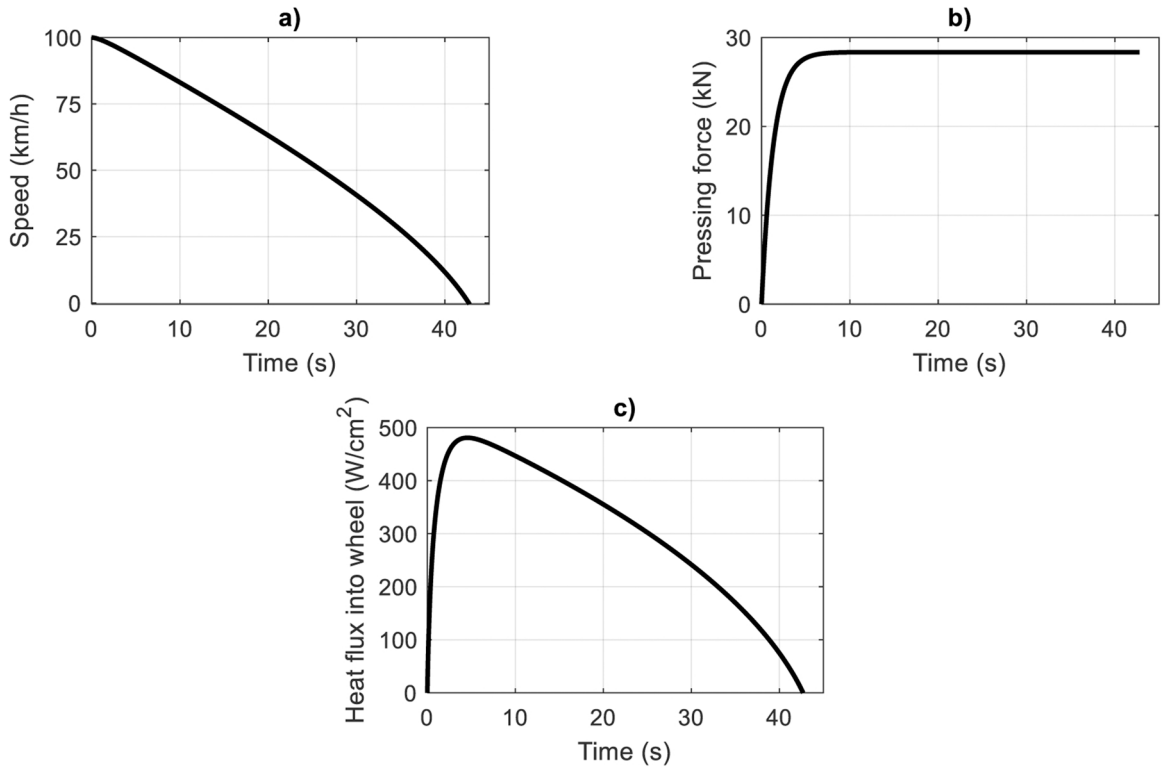

Fig. 9. Results of preliminary LTD simulation for stop braking of the reference freight wagon: a) speed profile; b) wheel-shoe pressing force and c) average heat flux flowing into the wheel at wheel-shoe contact.

axisymmetric model, i.e., a model that only considers the contribution of the 0-th order term in the Fourier series (2D HAE model in the plot legend). For the 2D HAE-NAL model, only useful harmonics up to 20-th order are retained, as the steady-state analysis shown in the lines above proves that good results can be obtained when the maximum retained order is at least equal to 15, see Fig. 8. For all models, Fig. 10 shows that the maximum temperature is not reached at the end of the stop braking operation, as temperature features an initial rise, then reaches a maximum and finally a decreasing trend is observed. This result is in line with the time history of heat flux as shown in Fig. 9c), since at the initial stage of the braking operation, the heat flux is high and temperature rises in a small portion of the wheel close to the outer surface. When the speed gets lower, internal conduction inside the wheel dominates over frictional heat flux and the temperature of the outer surface decreases.

The major difference among the temperature curves in Fig. 10 is that the 3D and 2D HAE-NAL curves have repeated heating and cooling during the stop braking operation, with temperature values that oscillate with respect to the curve corresponding to the 2D HAE temperature values. Therefore, the major results that can be inferred from Fig. 10 is that an excellent agreement exists between the outputs of the 2D HAE-NAL model and the results of the 3D model even for a transient simulation. However, it can be observed that the temperature oscillations for the 3D and 2D HAE-NAL models look irregular. This is because the step-size used for the simulations shown in Fig. 10 is equal to 10 ms, which does not allow to reach the convergence of the numerical integrator. However, this step-size is selected to compare the thermal models because, due to the huge computational and memory requirements, it was not possible to select a smaller step-size on the 3D model.

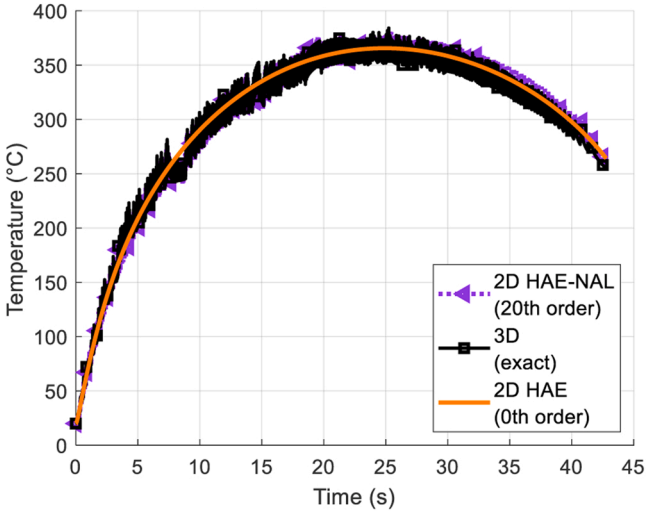

Fig. 10. Temperature evolution on a node in the middle of the tread calculated in the reference stop braking operation with step-size = 10 ms.

These irregular oscillations disappear if the step-size is refined, and this is evident from Fig. 11a), which shows the temperature time history obtained with a finer integration time-step of 2 ms. Obviously, since running a simulation using such a small value of time-step with the 3D model would lead to huge computational times and cause memory issues, only the results of the pure axisymmetric (2D HAE) model and 2D HAE-NAL model are plotted. From the zoom in Fig. 11b), which shows the temperature curves in a time interval corresponding to

Table 3
Main inputs for the FE simulation of transient stop braking operation.

Model Variable	Value	Unit
Ambient Temperature	20	°C
Initial temperature	20	°C
Stop Time	42.78	s
Initial speed	100	km/h
Convection coefficient	60	W/(m^2·K)
Wheelset lumped thermal capacitance	76552	J/K

approximately 5 wheel revolutions close to the instant when the maximum temperature is reached, it can be observed that, while the pure axisymmetric model is able to compute the average temperature trend only, the 2D HAE-NAL model predicts two temperature peaks for each revolution, which correspond to the instants when the node is in contact with the brake shoes, while cooling occurs for the remaining part of the revolution.

The main advantage of the 2D HAE-NAL model is clearly related to the computational efficiency, as considering an axisymmetric geometry leads to fewer nodes and hence DOFs. For the transient thermal analysis, the 3D model has a total of 975241 nodes, while the 2D HAE-NAL model only has 2495 nodes. The transient simulations are run on the same computer with Windows 11 Enterprise 64-bit (10.0, Build 22621) operating system (OS), AMD Ryzen 9 7950X processor (16 physical cores, 32 threads, clock frequency: 4.5 GHz, max turbo frequency: 5.7 GHz) and 32 GB of internal memory. For the 3D model, 2 cores are allocated for the simulation, and the total elapsed time for the solution is 97942 seconds, i.e., 27 hours and 12 minutes, which makes the simulation 2289 times slower than real-time. Conversely, for the 2D HAE-NAL model, the solution for a single harmonic contribution requires 62 seconds when run on a single thread when the step-size is set to 10 ms as for the 3D model, while 320 seconds (5 minutes and 20 seconds) are needed when a smaller step-size of 2 ms is set. Therefore, if proper parallel/distributed computing techniques are implemented, and the solution for each independent mode is calculated at the same time, the simulation with the 2D HAE-NAL model could be just 1.4 times slower than real-time with the large step-size (10 ms) and 7.2 times slower than real-time with a finer step-size (2 ms). Furthermore, it is important to remark that in addition to poor computational efficiency, the 3D model has memory issues, that limit the integrator time-step and can make it tricky to practically manage the model due to the large number of nodes.

4. Conclusions

Compared to existing axisymmetric models, the new 2D HAE-NAL model allows to calculate the temperature of tread-braked wheels considering the dependency of the thermal field on the circumferential coordinate, hence capturing the consequent heating-cooling cycles occurring during a wheel revolution. This is achieved by applying the Fourier series coefficient for the non-axisymmetric friction heat flux to the harmonic axisymmetric elements available from the ANSYS library.

Based on the results shown in the paper, it can be concluded that the 2D HAE-NAL model is validated and it is able to provide the same results as the reference 3D Workbench model in both steady-state and transient analyses. The steady-state simulations run at this stage of the activity suggest that the maximum retained harmonic order should be equal to 15 or higher to obtain results that agree with the outputs of the detailed 3D reference model. Therefore, the new 2D HAE-NAL model can effectively replace 3D modelling approaches when the variation of the temperature field along the circumferential coordinate is of interest, thus bringing great benefits in terms of computational efficiency. In fact, since it considers an axisymmetric geometry, the 2D HAE-NAL model has a lower number of nodes and DOFs, which speeds up the simulation and reduces the memory requirements for solution and output data storage.

Concerning the transient analysis run for the reference stop braking operation, when the same step-size of 10 ms is used, the 2D HAE-NAL model potentially requires only 62 seconds for the simulation, while the elapsed time for the 3D model is above 27 hours. Therefore, the new 2D HAE-NAL model can provide the same results as the 3D model with a reduction of computational times up to more than 3 orders of magnitude. Furthermore, since the 2D HAE-NAL model has lower memory and computational requirements compared to 3D model, it enables the definition of finer integration step-sizes. When the step-size is reduced by a factor 5 and set to 2 ms, the simulation with the 2D HAE-NAL model can potentially require only 320 seconds, thus leading to a speed up factor above 317 with respect to the 3D model, whilst at the same time ensuring a better numerical accuracy.

In view of its great accuracy and excellent computational efficiency when compared to 3D models, the developed 2D HAE-NAL model is suitable to be included within complex numerical frameworks modelling temperature-related phenomena, such as wheel tread wear and crack nucleation/propagation, thus providing a useful tool for the design of new shoe materials and braking systems, as well as for the optimization of maintenance operation planning and scheduling.

The major limitations of the developed 2D HAE-NAL model are related to the current incapability of accurately account for nonlinear phenomena, such as thermal radiation and the temperature-dependency of material parameters. Nonetheless, these limitations will be faced in future works with an “average” approach, namely considering the effects of nonlinearities only on the pure axisymmetric harmonic contribution.

In future upgrades of the activity, the authors are planning to experimentally tune and validate the developed thermal models against experimental data that will be collected from specifically designed twin-disc test benches. Since the activity shown in this paper proves that 2D HAE-NAL model provides the same output as the 3D model, the tuning of the model parameters will be performed on the 2D HAE-NAL model, that has superior computational performances. Furthermore, the 2D HAE-NAL model will serve as a reference for a further simplification aimed

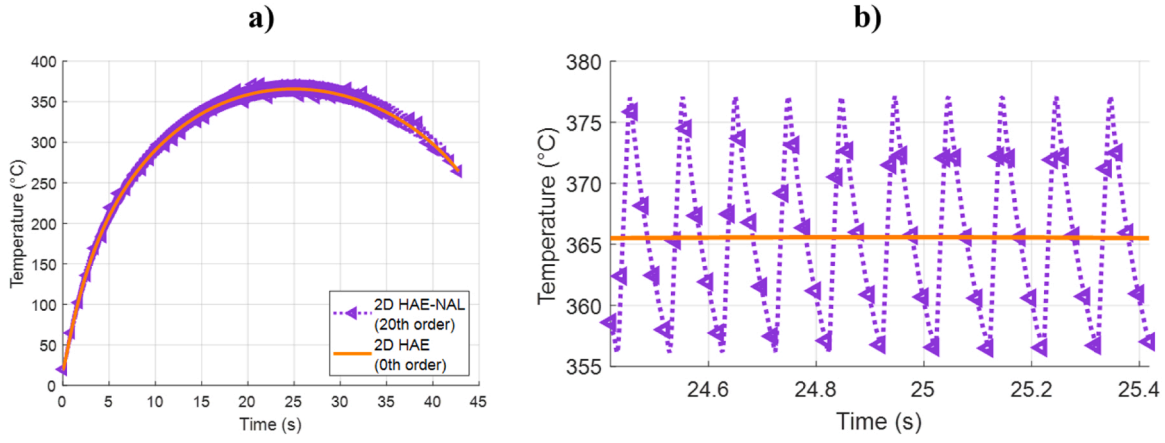

Fig. 11. Temperature evolution on a node in the middle of the tread calculated in the reference stop braking operation with step-size = 2 ms: a) time-history and b) zoom close to the time instant when the maximum temperature is reached. Please note that results of the 3D model are not given due to excessive computational burden.

at deriving a 1D thermal model, which is going to be implemented inside a MB package allowing to estimate the temperature field evolution inside tread braked wheels while at the same time simulating the railway vehicle dynamics. This will lead the path towards the simulation of the mutual dependency between thermal phenomena at the wheel-shoe contact and vehicle dynamics.

Declaration of Competing Interest

On behalf of all authors, the corresponding author states that there is nothing to declare.

Appendix A

The average frictional heat flux generated between the wheel and each block can be calculated from Eq. (A. 1) as:

$$\Phi^{*}_{tot}(t) = \mu_{wb}(v, F_N)v(t)\frac{F_N(t)}{A_{wb}} \tag{A. 1}$$

where t is time, μ_{wb} is the wheel-shoe friction coefficient, v is the wheel peripheral speed, F_N is the pressing force and A_{wb} is the contact area.

The amount of heat flux flowing towards the wheel Φ^* can be estimated through the definition of a partitioning factor (heat transfer coefficient) C_{ht} as stated by Eq. (A. 2):

$$\Phi^{*}(t) = C_{ht}\Phi^{*}_{tot}(t) \tag{A. 2}$$

The partitioning factor depends on the properties of the contacting bodies (wheel and shoes) and on their lateral surface. In this paper, the heat transfer coefficient is calculated according to the following literature expression [27,34], see Eq. (A. 3):

$$C_{ht} = \left\{1 + \left(\frac{\lambda_b\rho_b c_b}{\lambda_w\rho_w c_w}\right)^{\frac{1}{2}}\frac{A_b}{A_w}\right\}^{-1} \tag{A. 3}$$

where λ, ρ and c stand again for thermal conductivity, density and specific heat, A is used to indicate the lateral surface and finally subscripts b and w refer to block and wheel, respectively.

Appendix B

As stated by Equation (A.1), the friction heat flux depends on vehicle speed and wheel-block pressing force. In drag braking operations, speed and pressing force can be taken as constant, and the pressing force can be calculated from simple equilibrium considerations by superimposing the following identity as stated by Eq. (B. 1):

$$\mu_{wb}(v, F_N)F_N \bullet 2N_{ax}N_{bw} = M_{tot}gi_s \tag{B. 1}$$

where N_{ax} is the number of axles of the vehicle, N_{bw} is the number of blocks per vehicle, M_{tot} is the total mass of the wagon, g is gravity and finally i_s is the track slope. Please note that Equation (B.1.) considers the dependency of friction coefficient on speed and pressing force. In this paper, traditional P10 cast iron shoes are considered, for which the friction coefficient is estimated from Karwatzki's equation, see Eq. (B. 2):

$$\mu_{wb} = 0.6\frac{v + 100}{5v + 100}\frac{16/gF_N + 100}{80/gF_N + 100} \tag{B. 2}$$

where running speed and pressing force should be expressed in km/h and kN, respectively.

Shifting focus to sop braking, for such operations speed decreases to standstill, whilst the pressing force increases until filling the brake cylinder. The values of speed and pressing force can be estimated from LTD simulations. In this paper, stop braking operations of isolated wagons are concerned, however the method shown in the lines below can be easily extended to consider the LTD of full train compositions by including the modelling of in-train forces.

For the stop braking of an isolated vehicle, see Fig. B.1, the longitudinal equilibrium can be written as stated by Eq. (B. 3):

$$M_{tot}\ddot{s}(t) = -F_{air}(t) - F_{res}(t) \tag{B. 3}$$

where s is a curvilinear abscissa defining the position along the track, Fair is the total retarding force due to braking application and finally Fres corresponds to the resistant forces. The latter usually include the contribution of ordinary resistances as well as accidental resistances related to track slope and curvature. Since this paper only deals with braking operations on a straight level track, the resistant force coincides with the ordinary resistance, and it is calculated with the expression of the international benchmark of LTD simulators according to Eq. (B. 4):

$$F_{res} = F_{ord} = M_{tot} \bullet \left(2.943 + \frac{89.2}{P_{ax}} + 0.0306v + \frac{0.122v^2}{P_{ax}N_{ax}}\right) \tag{B. 4}$$

where P_{ax} is the vehicle axle-load in tonnes and speed and mass should be expressed in km/h and tonnes, respectively.

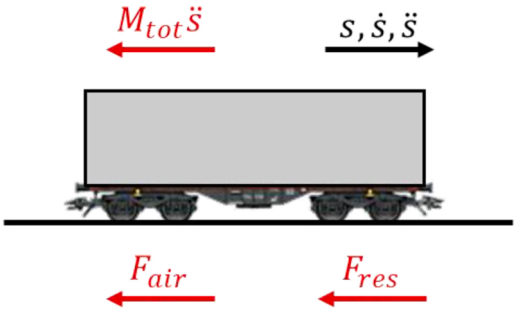

Figure B.1. Free body diagram of isolated braked wagon

The retarding forces due to braking can be estimated in each time step based on the applied pressing force as stated by Eq. (B. 5).

$$F_{air}(t) = \mu_{wb}(v, F_N)F_N(t) \bullet 2N_{ax}N_{bw} \tag{B. 5}$$

In this paper, the evolution of the pressing force is calculated with a heuristic law, assuming that pressure in the brake cylinder rises according to an exponential trend, using the following Eq. (B. 6):

$$F_N(t) = F_{N,\max} \bullet [1 - \exp(-t/\tau)] \tag{B. 6}$$

where $F_{N,max}$ corresponds to the maximum pressing force after filling the brake cylinder and τ is a model parameter that adjust the pressing force rise. The former depends on the main characteristics of the vehicle, while the latter is calculated by superimposing that the pressure in the brake cylinder reaches 95 % of its maximum value after a certain time t_{fill}, as stated by Eq. (B. 7).

$$\tau = \frac{t_{fill}}{\ln 20} \tag{B. 7}$$

Eqs. (B. 2)-(B. 7) are implemented to simulate the emergency stop braking of a reference vehicle whose main features are given in Annex O of the UIC 544–1 leaflet [50]. Table B.1 lists the main model parameters used in the simulations for the reference vehicle. Please note that the main non-linearities in the speed profile, see Fig. 9, are due to the nonlinear dependency of the wheel-shoe friction coefficient on speed and pressing force.

Table B.1
Model Parameters for the reference vehicle

Parameter Symbol	Variable description	Value	Unit
M_{tot}	Total weight on rails	80	ton
N_{ax}	Number of axles	4	-
N_{bw}	Number of blocks per wheel	2	-
P_{ax}	Axle-load	20	ton
$F_{N,max}$	Maximum pressing force	29.3	kN
t_{fill}	Brake cylinder filling time	4	s

Funding sources

This research did not receive any specific grant from funding agencies in the public, commercial, or not-for-profit sectors.

Declaration of Competing Interest

On behalf of all authors, the corresponding author states that there is nothing to declare.

Statement Originality

On behalf of all authors, the corresponding author hereby certifies that:

- the manuscript has not been published previously;
- the article is not under consideration for publication elsewhere;
- the article's publication is approved by all authors and tacitly or explicitly by the responsible authorities where the work was carried out.
- if accepted, the article will not be published elsewhere in the same form, in English or in any other language, including electronically, without the written consent of the copyright-holder.

Data availability

No data was used for the research described in the article.

References

[1] Teimourimanesh, S., Lundén, R. & Vernersson, T., Braking capacity of railway wheels—state-of-the-art survey. Presented at: *16th International Wheelset Congress (IWC16)*, Cape Town (South Africa), 14-19 March, 2010.

[2] Dedmon SL. Effect of temperature on the performance of railroad wheels. Proc Inst Mech Eng, Part F: J Rail Rapid Transit 2017;231(7):786–93. https://doi.org/10.1177/0954409717712072.

[3] Handa K, Kimura Y, Mishima Y. Surface cracks initiation on carbon steel railway wheels under concurrent load of continuous rolling contact and cyclic frictional heat. Wear 2010;268(1):50–8. https://doi.org/10.1016/j.wear.2009.06.029.

[4] Faccoli M, Ghidini A, Mazzù A. Changes in the Microstructure and Mechanical Properties of Railway Wheel Steels as a Result of the Thermal Load Caused by Shoe Braking. Metall Mater Trans A 2019;50(4):1701–14. https://doi.org/10.1007/s11661-019-05135-x.

[5] Faccoli M, Provezza L, Petrogalli C, Ghidini A, Mazzù A. Effects of full-stops on shoe-braked railway wheel wear damage. Wear 2019;428-429:64–75. https://doi.org/10.1016/j.wear.2019.03.006.

[6] Ikeuchi K, Handa K, Lundén R, Vernersson T. Wheel tread profile evolution for combined block braking and wheel–rail contact: Results from dynamometer experiments. Wear 2016;366-367:310–5. https://doi.org/10.1016/j.wear.2016.07.004.

[7] Walia MS, Esmaeili A, Vernersson T, Lundén R. Thermomechanical capacity of wheel treads at stop braking: A parametric study. Int J Fatigue 2018;113:407–15. https://doi.org/10.1016/j.ijfatigue.2018.04.031.

[8] Fec MC, Sehitoglu H. Thermal-mechanical damage in railroad wheels due to hot spotting. Wear 1985;102(1):31–42. https://doi.org/10.1016/0043-1648(85)90089-4.

[9] Kwon SJ, Lee DH, Kwon ST, Goo BC. Failure analysis of railway wheel tread. Key Eng Mater 2006;321:649–53.

[10] Moyar GJ, Stone DH. An analysis of the thermal contributions to railway wheel shelling. Wear 1991;144(1):117–38. https://doi.org/10.1016/0043-1648(91)90010-R.

[11] Stone, D., An Interpretive Literature Review of Wheel Shelling. ASME 2008 Rail Transportation Division Fall Technical Conference, pp. 149-155, 2008. https://doi.org/10.1115/rtdf2008-74028.

[12] Srivastava JP, Sarkar PK, Ranjan V. Effects of thermal load on wheel–rail contacts: A review. J Therm Stress 2016;39(11):1389–418. https://doi.org/10.1080/01495739.2016.1216060.

[13] Vakkalagadda MRK, Srivastava DK, Mishra A, Racherla V. Performance analyses of brake blocks used by Indian Railways. Wear 2015;328-329:64–76. https://doi.org/10.1016/j.wear.2015.01.044.

[14] Cantone L, Ottati A. Modelling of friction coefficient for shoes type LL by means of polynomial fitting. Open Transp J 2018;12(1).

[15] Vernersson T. Thermally induced roughness of tread-braked railway wheels: Part 1: brake rig experiments. Wear 1999;236(1):96–105. https://doi.org/10.1016/S0043-1648(99)00260-4.

[16] Stojanovic N, Glisovic J, Abdullah OI, Belhocine A, Grujic I. Particle formation due to brake wear, influence on the people health and measures for their reduction: a review. Environ Sci Pollut Res 2022;29(7):9606–25. https://doi.org/10.1007/s11356-021-17907-3.

[17] Stojanovic N, Belhocine A, Abdullah OI, Grujic I. The influence of the brake pad construction on noise formation, people's health and reduction measures. Environ Sci Pollut Res 2023;30(6):15352–63. https://doi.org/10.1007/s11356-022-23291-3.

[18] Stojanovic, N., Igrutinovic, S., Belhocine, A., Boskovic, B. & Grujic, I., The composition, working parameters and measures for the brake wear reduction: A review. *Proceedings of the Institution of Mechanical Engineers, Part J: Journal of Engineering Tribology*, 0(0), pp. 13506501241291393, https://doi.org/10.1177/13506501241291393.

[19] Magelli M, Zampieri N, Wu Q. Integration of brake block thermal equations within a railway vehicle multibody model: a multiphysics approach. Int J Rail Transp 2024:1–16. https://doi.org/10.1080/23248378.2023.2301618.

[20] Wu Q, Magelli M, Zampieri N, Bernal E. Adding a brake shoe temperature model into freight train longitudinal braking dynamics simulations. Proc Inst Mech Eng, Part F: J Rail Rapid Transit 2023;237(5):631–41. https://doi.org/10.1177/09544097221126274.

[21] Wu Q, Spiryagin M, Cole C. Block–Wheel–Rail Temperature Assessments Via Longitudinal Train Dynamics Simulations. J Comput Nonlinear Dyn 2022;17(11). https://doi.org/10.1115/1.4055431.

[22] Tudor A, Khonsari MM. Analysis of Heat Partitioning in Wheel/Rail and Wheel/Brake Shoe Friction Contact: An Analytical Approach. Tribology Trans 2006;49(4):635–42. https://doi.org/10.1080/10402000600927886.

[23] Siniscalchi, R. & Cantone, L., Two fast models to compute the thermal field in wagons with brake blocks via finite differences. *Proceedings of the Institution of Mechanical Engineers, Part F: Journal of Rail and Rapid Transit*, 0(0), pp. 09544097241308113, https://doi.org/10.1177/09544097241308113.

[24] Vernersson T. Temperatures at railway tread braking. Part 1: Modelling. Proc Inst Mech Eng, Part F: J Rail Rapid Transit 2007;221(2):167–82. https://doi.org/10.1243/0954409JRRT57.

[25] Vernersson T. Temperatures at railway tread braking. Part 2: calibration and numerical examples. Proc Inst Mech Eng, Part F: J Rail Rapid Transit 2007;221(4):429–41. https://doi.org/10.1243/09544097jrrt90.

[26] Vernersson T, Lundén R. Temperatures at railway tread braking. Part 3: wheel and block temperatures and the influence of rail chill. Proc Inst Mech Eng, Part F: J Rail Rapid Transit 2007;221(4):443–54. https://doi.org/10.1243/09544097jrrt91.

[27] Vakkalagadda MRK, Vineesh KP, Racherla V. Estimation of railway wheel running temperatures using a hybrid approach. Wear 2015;328-329:537–51. https://doi.org/10.1016/j.wear.2015.03.026.

[28] Teimourimanesh S, Vernersson T, Lundén R. Modelling of temperatures during railway tread braking: Influence of contact conditions and rail cooling effect. Proc Inst Mech Eng, Part F: J Rail Rapid Transit 2014;228(1):93–109. https://doi.org/10.1177/0954409712465696.

[29] Suresh Babu A, Siva Prasad N. Coupled field finite element analysis of railway block brakes. Proc Inst Mech Eng, Part F: J Rail Rapid Transit 2009;223(4):345–52. https://doi.org/10.1243/09544097JRRT256.

[30] Bosso N, Cantone L, Falcitelli G, Gjini R, Magelli M, Nigro FM, et al. Simulation of the thermo-mechanical behaviour of tread braked railway wheels by means of a 2D finite element model. Tribology Int 2023;178. https://doi.org/10.1016/j.triboint.2022.108074.

[31] Milošević M, Stamenković D, Tomić M, Milojević A, Mijajlović M. Modeling thermal effects in braking systems of railway vehicles. *Therm Sci,* 16(2) 2012:515–26. https://doi.org/10.2298/TSCI120503188M.

[32] Pradhan S, Samantaray AK. A Recursive Wheel Wear and Vehicle Dynamic Performance Evolution Computational Model for Rail Vehicles with Tread Brakes. Vehicles 2019;1(1):88–115. https://doi.org/10.3390/vehicles1010006.

[33] Haidari A, Hosseini-Tehrani P. Fatigue Analysis of Railway Wheels Under Combined Thermal and Mechanical Loads. J Therm Stress 2014;37(1):34–50. https://doi.org/10.1080/01495739.2013.850967.

[34] Haidari A, Tehrani PH. Thermal load effects on fatigue life of a cracked railway wheel. Lat Am J Solids Struct 2015;12:1144–57. https://doi.org/10.1590/1679-78251658.

[35] Yevtushenko A, Kuciej M, Grzes P, Wasilewski P. Methodology of estimation of temperature mode in the 2xBgu type railway braking system. Sci Rep 2022;12(1). https://doi.org/10.1038/s41598-022-25283-2.

[36] Yevtushenko AA, Grzes P. Axisymmetric FEA of temperature in a pad/disc brake system at temperature-dependent coefficients of friction and wear. Int Commun Heat Mass Transf 2012;39(8):1045–53. https://doi.org/10.1016/j.icheatmasstransfer.2012.07.025.

[37] Xia YM, Guo B, Cong GQ, Zhang XH, Zeng GY. Numerical simulation of rock fragmentation induced by a single TBM disc cutter close to a side free surface. Int J Rock Mech Min Sci 2017;91:40–8. https://doi.org/10.1016/j.ijrmms.2016.11.004.

[38] Su W, Li X, Jin D, Yang Y, Qin R, Wang X. Analysis and prediction of TBM disc cutter wear when tunneling in hard rock strata: A case study of a metro tunnel excavation in Shenzhen, China. Wear 2020;446-447:203190. https://doi.org/10.1016/j.wear.2020.203190.

[39] Xia Y, Yin X, Fu J, Liu Y, Cui J, Zhang H. Study on the distribution and variation of temperature field in the rock breaking process of TBM disc cutter. Int J Therm Sci 2023;186:108086. https://doi.org/10.1016/j.ijthermalsci.2022.108086.

[40] Magelli M, Pagano R, Zampieri N. Design of an Innovative Twin-Disc Device for the Evaluation of Wheel and Rail Profile Wear. Designs 2024;8(4):73.

[41] Belhocine A, Abdullah OI. Finite element analysis (FEA) of frictional contact phenomenon on vehicle braking system. Mech Based Des Struct Mach 2022;50(9):2961–96. https://doi.org/10.1080/15397734.2020.1787843.

[42] Belhocine A, Shinde D, Patil R. Thermo-mechanical coupled analysis based design of ventilated brake disc using genetic algorithm and particle swarm optimization. JMST Adv 2021;3(3):41–54. https://doi.org/10.1007/s42791-021-00040-0.

[43] ANSYS Mechanical, Release 2021R2, Theory reference, ANSYS, Inc.

[44] ANSYS Mechanical APDL Element Reference, Release 14.0, ANSYS, Inc. 2011.

[45] Yuan Z, Tian C, Wu M, Wang G. A modified uniformly distributed heat source method for predicting braking temperature of railway brake disc. Int J Rail Transp 2022;10(2):216–29. https://doi.org/10.1080/23248378.2021.1882890.

[46] Zewang Y, Chun T, Mengling W, Jiajun Z, Chao C. Modeling and Model Validation of Thermal Behavior of Railway Disc During Single Braking. J Therm Sci Eng Appl 2021;13(5). https://doi.org/10.1115/1.4049984.

[47] Deressa KT, Ambie DA. Non-axisymmetric Modeling of a Moving Heat Source for Thermal Stress and Fatigue Analysis of Railway Vehicle Disc Brakes. Urban Rail Transit 2024;10(1):42–64. https://doi.org/10.1007/s40864-023-00207-z.
[48] Grzes P. Adaptation of rectangular and trapezoidal time functions to simulate the rotational motion of the brake disc. Mech Syst Signal Process 2024;207:110923. https://doi.org/10.1016/j.ymssp.2023.110923.
[49] Commission Regulation (EU) No 321/2013 of 13 March 2013 concerning the technical specification for interoperability relating to the subsystem 'rolling stock — freight wagons' of the rail system in the European Union and repealing Decision 2006/861/EC. 2013.
[50] UIC 544-1:2014. *Brakes - Braking power*.
[51] Bosso N, Magelli M, Zampieri N. A numerical method for the simulation of freight train emergency braking operations based on the UIC braked weight percentage. Railw Eng Sci 2023. https://doi.org/10.1007/s40534-022-00296-9.
[52] Bosso N, Magelli M, Rossi Bartoli L, Zampieri N. The influence of resistant force equations and coupling system on long train dynamics simulations. Proc Inst Mech Eng, Part F: J Rail Rapid Transit 2022;236(1):35–47. https://doi.org/10.1177/09544097211001149.
[53] Bosso N, Magelli M, Zampieri N. Long train dynamic simulation by means of a new in-house code. In: Passerini G, Mera JM, Takagi R, editors. *WIT Transactions on the Built Environment* **199**. Southampton (UK): WIT Press; 2020. p. 249–59. https://doi.org/10.2495/CR200231.
[54] Bosso N, Magelli M, Zampieri N. Validation of a new longitudinal train dynamics code for time domain simulations and modal analyses. Int J Transp Dev Integr 2021;5(1):41–56. https://doi.org/10.2495/TDI-V5-N1-41-56.